Neurobiology of Disease

# Skeletal Muscle $IP_3R_1$ Receptors Amplify Physiological and Pathological Synaptic Calcium Signals

**Haipeng Zhu,[1] Bula J. Bhattacharyya,[2] Hong Lin,[3] and Christopher M. Gomez[1]**

[1]Department of Neurology, University of Chicago Medical Center, Chicago, Illinois 60637, [2]Department of Molecular Pharmacology and Biological Chemistry, Feinberg School of Medicine, Northwestern University, Chicago, Illinois 60611, and [3]Departments of Neurology and Pediatrics, the Children's Hospital of Philadelphia, Philadelphia, Pennsylvania 19104-4318

**$Ca^{2+}$ release from internal stores is critical for mediating both normal and pathological intracellular $Ca^{2+}$ signaling. Recent studies suggest that the inositol 1,4,5-triphosphate ($IP_3$) receptor mediates $Ca^{2+}$ release from internal stores upon cholinergic activation of the neuromuscular junction (NMJ) in both physiological and pathological conditions. Here, we report that the type I $IP_3$ receptor ($IP_3R_1$)-mediated $Ca^{2+}$ release plays a crucial role in synaptic gene expression, development, and neuromuscular transmission, as well as mediating degeneration during excessive cholinergic activation. We found that $IP_3R_1$-mediated $Ca^{2+}$ release plays a key role in early development of the NMJ, homeostatic regulation of neuromuscular transmission, and synaptic gene expression. Reducing $IP_3R_1$-mediated $Ca^{2+}$ release via siRNA knockdown or $IP_3R$ blockers in C2C12 cells decreased calpain activity and prevented agonist-induced acetylcholine receptor (AChR) cluster dispersal. In fully developed NMJ in adult muscle, $IP_3R_1$ knockdown or blockade effectively increased synaptic strength at presynaptic and postsynaptic sites by increasing both quantal release and expression of AChR subunits and other NMJ-specific genes in a pattern resembling muscle denervation. Moreover, in two mouse models of cholinergic overactivity and NMJ $Ca^{2+}$ overload, anti-cholinesterase toxicity and the slow-channel myasthenic syndrome (SCS), $IP_3R_1$ knockdown eliminated NMJ $Ca^{2+}$ overload, pathological activation of calpain and caspase proteases, and markers of DNA damage at subsynaptic nuclei, and improved both neuromuscular transmission and clinical measures of motor function. Thus, blockade or genetic silencing of muscle $IP_3R_1$ may be an effective and well tolerated therapeutic strategy in SCS and other conditions of excitotoxicity or $Ca^{2+}$ overload.**

## Introduction

Dysregulation of $Ca^{2+}$ release from internal stores is increasingly recognized as a potential cause of neuronal death or neurodegeneration (Demuro et al., 2010; Bezprozvanny, 2011). Therefore, one potential therapeutic strategy to prevent pathological elevations of $Ca^{2+}$ may be pharmacological inhibition of internal $Ca^{2+}$ release, provided that the effect on normal physiological signaling is tolerated. For example, malignant hyperthermia, a condition of ryanodine receptor overactivity and pathological elevation of muscle $Ca^{2+}$, can be successfully treated by pharmacological blockade of the ryanodine receptor (Kobayashi et al., 2009).

The inositol 1,4,5-triphosphate ($IP_3$) receptor ($IP_3R$) channel initiates a slow wave of internal store $Ca^{2+}$ release, often at specific subcellular locations, that allows compartmentalization of $Ca^{2+}$ signals within cells (Marks, 1997). $IP_3Rs$ are gated by the combined binding of $IP_3$ generated by the hydrolysis of phospholipids by phospholipase C and by $Ca^{2+}$, which enters through AChR or voltage-gated channels (Streb et al., 1983; Berridge and Irvine, 1984). Type 1 ($IP_3R_1$) is the most abundant and best studied of the three subtypes of $IP_3R$. The gene encoding $IP_3R_1$, *itpr1*, is highly expressed in cerebellar Purkinje neurons and cardiac and skeletal muscle and is highly concentrated at the neuromuscular junction (NMJ) and the subsynaptic nuclei (Furuichi et al., 1990; Ross et al., 1992; Powell et al., 2003).

The discrete localization of $IP_3R_1$ near the acetylcholine (ACh) receptors (AChRs) and in postsynaptic areas surrounding NMJ nuclei is striking and suggests a role for $IP_3R_1$-mediated $Ca^{2+}$ release in synaptic gene expression and synaptic physiology in muscle (Powell et al., 2003). Focal iontophoresis of ACh onto endplates of dissociated, fura-2-loaded muscle fibers induces localized increases in NMJ $Ca^{2+}$ that depend on functioning $IP_3Rs$ (Zayas et al., 2007). Therefore, because $IP_3Rs$ amplify postsynaptic $Ca^{2+}$ signals at NMJs and because $Ca^{2+}$ is critical for postsynaptic changes leading to early development and maturation of the NMJ, we postulate that $IP_3R_1s$ are required to mediate the effects of cholinergic input on NMJ development *and function (Zhu and Peng, 1988; Megeath and Fallon, 1998).

$Ca^{2+}$ also mediates the effects of cholinergic excess at the NMJ, such as in myopathy caused by excessive anti-cholinesterase medication (agonist myopathy), congenital myasthenic syndromes, and insecticide poisoning (Kawabuchi, 1982; Engel et al., 2010). The

Received July 22, 2011; revised Aug. 24, 2011; accepted Sept. 1, 2011.

Author contributions: H.Z., B.J.B., H.L., and C.M.G. designed research; H.Z., B.J.B., H.L., and C.M.G. performed research; H.Z. contributed unpublished reagents/analytic tools; H.Z., B.J.B., H.L., and C.M.G. analyzed data; H.Z., B.J.B., H.L., and C.M.G. wrote the paper.

This work is supported by NIH Grant RO1 NS33202 (C.M.G.).We thank Katherine Hekman for helpful comments in preparing this manuscript.

The authors declare no competing financial interests.

Correspondence should be addressed to Dr. Christopher M. Gomez, Department of Neurology, Albert Merritt Billings Hospital S237, MC2030, University of Chicago Medical Center, 5841 South Maryland, Chicago, IL 60637. E-mail: gomez001@uchicago.edu.

DOI:10.1523/JNEUROSCI.3766-11.2011

 0270-6474/11/3115269-15$15.00/0

slow-channel congenital myasthenic syndrome (SCS) is caused by mutations in the muscle AChR channel leading to $Ca^{2+}$ overload and degeneration of the NMJ (Gomez et al., 2002). Elevated postsynaptic $Ca^{2+}$ in SCS requires entry of $Ca^{2+}$ through ACh-activated mutant AChR channels and release of $Ca^{2+}$ from $IP_3$-gated stores (Zayas et al., 2007). We hypothesized that $IP_3R_1$ mediates developmental and physiological events localized to the NMJ, as well as pathological sequelae from cholinergic excess at the NMJ. We show that $IP_3R_1$s are required to mediate cholinergic signals responsible for AChR cluster dispersal, homeostatic plasticity, and synaptic gene expression at the NMJ. However, blockade of $IP_3R$ or specific knockdown of $IP_3R_1$ in adult muscle prevents the excitotoxic effects of cholinergic excess and pathological synaptic $Ca^{2+}$ overload without impacting normal NMJ function. Thus, a therapeutic strategy targeted to block muscle $IP_3R_1$ is likely to be well tolerated.

## Materials and Methods

*Materials*. Chemical reagents were purchased from Sigma. Cell culture materials were obtained from Invitrogen . Laminin, alpha-bungarotoxin ($\alpha$BT)-conjugated Texas Red (TxR-$\alpha$BT), and fluorescence-tagged secondary antibody were purchased from Invitrogen. Secondary antibodies with horseradish peroxidase (HRP) were provided by GE Healthcare Bioscience. GFP-tagged control siRNA was purchased from Santa Cruz Biotechnology Primary antibodies were used against the following targets: neural filament (1:1000; Abcam), phosphorylated H2AX (Ser139; 1:500; Millipore), cleaved caspase 3 and 9 (1:200;Cell Signaling Technology), synaptophysin (1:500; Cell Signaling Technology), S100 (1:100; Abcam), histone deacetylase 4 (HDAC4; 1:500; Abcam), glial fibrillary acidic protein (1:500; Cell Signaling Technology), fibronectin (1:500; Abcam), $IP_3R_1$ (1:500; Alomone), and glyceraldehyde 3-phosphate dehydrogenase (GAPDH; 1:5000; Ambion).

*Plasmid and construct assembly*. Mouse INPP5a (inositol polyphosphate-5-phosphatase) cDNA, purchased from Thermo Scientific (Open Biosystems), was cloned into pEGFP-N1 (Clontech).

*Cell culture*. C2C12 cells purchased from American Tissue Culture Collection (Manassas, VA) were cultured and differentiated on poly-L-lysine and laminin-coated plates as described previously (Sugiyama et al., 1997). After 72–96 h, C2C12 cells were incubated with calcium ($Ca^{2+}$; 100 $\mu$M), carbachol (CCh; 100 $\mu$M), 2-aminoethoxydiphenyl borate (2-APB; 100 $\mu$M), or xestospongin C (XS; 10 $\mu$M) for 15 min, washed 3× with culture medium, and then incubated at 37°C and sampled for fluorescence at intervals up to 120 min. Cover slides were washed and prepared for cytofluorescence. Cells were transfected with siRNA and scrambled RNA (ctRNA) segments using lipofection (Lipofectamine 2000, Invitrogen).

*Animals and tissue preparation*. Four- to six-month-old male wild-type FVB mice and SCS transgenic mice ($\varepsilon$L269F) were used in this study (Gomez et al., 1997). All drug treatments and surgical procedures followed the animal care and use protocols established by the Institutional Animal Care and Use Committee (University of Chicago, Chicago, IL). Mice were anesthetized using ketamine and xylazine (Mulder and Mulder, 1979). For denervation, hind limbs of anesthetized mice were shaved to expose skin over the sciatic nerve. Segments of the sciatic nerve (1 cm) were excised, and the two free nerve trunks were physically separated within the muscle before wounds were closed with stainless steel wound clips.

*Drug administration*. Neostigmine methylsulfate and 2-APB in saline (USP) were administered intraperitoneally at 250 $\mu$g/kg for 36 h and 10 mg/kg/8 h for 9 d, respectively (Carlson and Kriebel, 1985; Bootman et al., 2002). XS (5 nM) in DMSO was injected intraperitoneally into mice every 2 h for 12 h (Galeotti et al., 2006). $\alpha$BT (1 mg/ml; Tocris Bioscience) in saline was injected intraperitoneally at a dose of 0.5 $\mu$g/d for 6 d (Holland and Brown, 1980; Domet et al., 1995). Control tibialis anterior (TA) muscle was treated with DMSO or saline (0.9% w/v; USP) as control.

*RNA extraction, cDNA synthesis, and real-time PCR*. TA muscle was homogenized in tri-reagent (Sigma) to extract total RNA, which was used (1 $\mu$g) to synthesize cDNA (First-Strand Synthesis Kit; Invitrogen). Assay conditions for real-time PCR were adjusted for each single target using melt curve analysis and gel electrophoresis with specific primers (Table 1) and SYBR Green (Bio-Rad). To minimize variation, all sequences of interest were amplified in parallel from one aliquot of cDNA on the same plate. Real-time PCR was performed on iCycler iQ Real-Time PCR Detection System (Bio-Rad) following the manufacturer's instructions, with GAPDH used as a housekeeping gene. The mean value from triplicate samples generated from the same RNA preparation was used to determine the real-time PCR efficiency (dilution rates: 1:3; 1:9; 1:27; 1:81; 1:243; 1:729) for each gene with the slope of a linear regression model. The data with efficiency (≥98.5%) were selected as valid results.

**Table 1. Primers and siRNA sequences**

| Gene name | Sense primer | Antisense primer |
|---|---|---|
| nAChR$\alpha$ | CTGTTCTCCTGCTGCTAGGC | AGCTGTAGACCCACGGTGAC |
| nAChR$\gamma$ | TTCGATTGGCAGAACTGTTCC | ATTTTACGAGGACCTGAGGCA |
| nAChR$\sigma$ | ATCTCCCTGAAAGAAGTGGAGGAGA | GAACGAGCCATCATTGTTGTTCTCCA |
| nAChR$\epsilon$ | CTCATTTTTCGCTCCCAGAC | TGTGGAACCTCCCTCATAGC |
| ErbB-2 | CCTGCCTCCACTTCAATCAT | CAGAGTGCAGGATCCCACTT |
| MuSK | GGACAATGCTCTCAGGGAAA | TAGCGTCCTGCTCAGGTTCT |
| Rapsyn | GACTATGGCAAAGGCTGGAG | ATATCGGCAAAGCAGAGCAG |
| HDAC-4 | AGTTCTCACTGCCCTTGGAA | TCCTGCTGCTGCTTGATATG |
| Myogenin | AACCAGGAGGAGCGCGATCT | TCTGCGGGTGTTAGACGTGAG |
| Dach-2 | TGAAACTTTGTTCACCGATTG | TTCTACTTCGAATACCGTTACT |
| AChE | TATGCCTACATCTTTGAACACCGTGC | GAGATTTGGAGTCTCGAGGGTCATT |
| Glut1 | CCAACAGCTCTCAGGCATCAATGCT | CAAATATGGCCACGATGGAGACATAG |
| Glut4 | TACTACTCAACGAGCATCTTCGAGAA | ACGATGCTCAGATAGGACATCCAA |
| IP3R1 | siRNA | |
| Sequence 1 | AACATTGTGCAGAAAACAGCC | |
| Sequence 2 | AACAAAGAGATCCGTAGTAAG | |

MuSK, Muscle-specific receptor tyrosine kinase; ErbB-2, erythroblastic leukemia viral oncogene homolog 2; HDAC-4, histone deacetylase 4; Dach-2, Dachshund2; nAChR$\alpha$, $\alpha$ subunit of acetylcholine receptor; nAChR$\gamma$, $\gamma$ subunit of acetylcholine receptor; nAChR$\sigma$, $\sigma$ subunit of acetylcholine receptor; nAChR$\epsilon$, $\epsilon$ subunit of acetylcholine receptor; AChE, acetylcholine esterase; Glut1 and 4, glucose transporters 1 and 4.

*Western blotting*. Tissue was homogenized in 50 mM Tri-HCl, pH 7.6, 150 mM NaCl, 1% SDS, 1% Triton X-100, 0.1 mM EGTA, and 0.1 mM EDTA supplemented with a (Roche Protease Inhibitor Cocktail. Homogenates were fractionated by SDS-PAGE and transferred onto a nitrocellulose membrane (Bio-Rad). Membranes were blocked for 1 h in TBS-T (50 mM Tris-HCl, pH 7.4, 150 mM NaCl, and 0.05%Tween-20) containing 5% nonfat milk and then incubated overnight with primary antibodies. After 3× wash in TBS-T, the membrane was incubated with HRP-conjugated secondary antibody for 1 h and washed again 3×. Immunolabeled bands were developed using ECL reagents (Ambion) on x-ray film. Reaction product levels were quantified by scanning densitometry using NIH ImageJ (version 5.3).

*Cell and tissue staining and imaging*. For cytofluorescence, cells grown on coverslips were fixed in methanol-acetone (−20°C × 20 min) and blocked with blocking solution (3% normal goat serum, 0.3% Triton X-100, 1 h at room temperature). TxR-$\alpha$BT (1:500; Molecular Probes) was used to detect AChRs. Motor endplates were localized and $Ca^{2+}$-overloaded endplates were detected in cryosections using histochemical stains for cholinesterase and $Ca^{2+}$ [glyoxal-bis(2-hydroxyanil) (GBHA)] as described previously (Koelle and Friedenwald, 1949; Kashiwa and House, 1964). For immunohistochemistry, tissue sections were fixed by methanol-acetone at −20°C for 30 min, air dried for 20 min, and incubated with blocking solution for 1 h at room temperature, followed by overnight incubation with primary antibody at 4°C. After washing, the sections were incubated with fluorescent secondary antibody in PBS-T (phosphate buffered saline and 0.05% Tween 20) for 1 h at room temperature. Confocal fluorescence microscopy was carried out under a TCS laser scanning microscope (Leica). Optical sections of 0.5 $\mu$m were scanned at the *z*-axis. ImageJ was used to quantify the percentage of labeling by specific antibody in NMJs of each sample.

*Quantitative studies in tissue sections*. Quantitation of the proportion of labeled NMJs in limb muscle cryosections was carried out using sequential alternate sections stained for cholinesterase or test labeled (GBHA,

pH2X, and HDAC4) as described previously (Gomez et al., 1997, 2002) employing ImageJ (version 5.3).

*Calpain and caspase activity assay*. Calpain, caspase-3, and caspase-9 activities in muscle or cell homogenates were measured using a firefly luciferase-based assay (Calpain-Glo Protease Assay, Caspase-Glo 3/7 Assay, or Caspase-Glo 9 Assay; Promega). Cell and muscle tissue were homogenized as described previously (Lee et al., 2008), except for the addition of 10 mM $NH_4Cl$ and 10 mM 3-methyladenine to the homogenization buffer to stabilize lysosomes and the proteosome. Protein samples (20 $\mu$g) were analyzed by luminometer (Turner BioSystems) in triplicate.

*Intramuscular electroporation-mediated gene delivery*. Electroporation of plasmid and siRNA were carried out as described previously (Schertzer et al., 2006). Briefly, after anesthesia the legs were shaved and the TA muscles were injected with hyaluronidase (30 $\mu$l; Sigma-Aldrich) 2 h before performing electroporation. Subsequently, 10 $\mu$g of optimal siRNA segments, control RNA, or expression plasmids in saline were injected into the TA muscle. Immediately following injection, 10 separate electrical pulses (10 ms) were delivered through circle electrodes (1 cm diameter) applied to the ventral and dorsal surfaces flanking the TA at 175 V/cm with 1 Hz via a square-wave electroporator (ECM830; Harvard Apparatus).

*Electromyography and* in vitro *electrophysiology*. Compound muscle action potentials (CMAPs) were detected and calculated as described previously using a Nicolet VikingQuest (Nicolet Biomedical) (Groshong et al., 2007).

*Voltage-clamp studies*. All experiments were carried out *in vitro* at room temperature on the sciatic nerve and tibialis muscle preparations of 5–6 week-old mice. For dissection, mice were deeply anesthetized with isofluorane. The tibialis anterior muscle was dissected free from the extensor digitorum longus (EDL) muscle, partially bisected, and folded apart to flatten the muscle before pinning it down. Because the sciatic nerve innervates both EDL and TA muscles, we transected the EDL and posterior portion of the TA muscle to eliminate excessive muscle contraction. To prevent muscle action potentials, $\mu$-conotoxin GIIIB (2 $\mu$M) was included in some experiments.

The TA muscle was perfused with Tyrode's solution (137 mM NaCl, 2.8 mM KCl, 1.8 mM $CaCl_2$, 1.1 mM $MgCl_2$, 11.9 mM $NaHCO_3$, 0.33 mM $NaH_2PO_4$, and 11.2 mM dextrose, pH 7.4, when bubbled with a mixture of 95% $O_2$ and 5% $CO_2$) at 30°C. Intracellular potentials and currents were measured using an Axoclamp-2A amplifier system and glass microelectrodes filled with 3 M KCl (resistance, 10–15 M$\Omega$). Using the two-microelectrode voltage-clamp system, synaptic currents, including miniature endplate currents (MEPCs) and endplate currents (EPCs), were obtained at −70 mV holding potential. The currents were digitized at 50 $\mu$s per point and stored, captured, and analyzed using pClamp9 software (Molecular Devices). EPCs were elicited by stimulating the corresponding sciatic nerve with rectangular pulses of 0.05 ms duration. During single shock stimulation, the nerve was stimulated at 0.2 Hz. The amplitude decay and time to peak of the EPCs and MEPCs were captured and subsequently analyzed with pClamp 9.2 and the Mini Analysis Program (Synaptosoft). Quantal content was determined by dividing MEPC amplitude with EPC amplitude from the same endplate (Bhattacharyya et al., 1997; Wilson et al., 2002; Groshong et al., 2007).

*Treadmill gait analysis*. Mouse gait analysis was performed via the DigiGait Imaging System (Mouse Specifics) as described previously (Hampton et al., 2004; Gómez-Sintes and Lucas, 2010). Briefly, mice walked on a motor-driven treadmill with a transparent treadmill belt. A high frame rate camera was focused on the ventral plane of the mice as they walked within an acrylic chambe, ~5 cm wide by ~25 cm long. The areas of the approaching or retreating paws relative to the belt and camera were calculated throughout each stride. Plotting the area of each paw in time provides a dynamic gait signal, representing the temporal record of paw placement relative to the treadmill belt. Each gait signal for each limb comprises a stride duration (stride time), which includes the stance duration when the paw of a limb was in contact with the treadmill, plus the swing duration when the paw of the same limb was not in contact with the treadmill belt. Stance duration is comprised of a braking time (increasing paw contact area over time) and propulsion time (decreasing paw contact area over time). Stride frequency was calculated by counting the number of gait signals over time. Stride length was calculated from the equation: speed = stride frequency × stride length. Due to the remarkable reduction of muscle strength in SCS mice, brake time was primarily selected as the most sensitive metric to demonstrate functional improvement of treated muscle in SCS mice. The walking speed was set to 25 cm/s. Approximately 5 s of video were collected for each walking subject to provide ~20 sequential strides.

*Statistics*. Values were represented as the mean ± SD. Data were analyzed using a Student's *t* test, where appropriate, and a nonparametric Mann–Whitney *U* test, for comparison of percentages and ratio values, as indicated in figure legends.

## Results

### $IP_3R_1$ mediates cholinergic agonist-induced dispersal of AChR clusters in myogenic cells

In normal muscle cells and C2C12 myogenic cells, stimulation of AChRs with cholinergic agonists causes a transient increase in cytoplasmic $Ca^{2+}$ levels and dispersal of agrin- or laminin-induced AChR clusters in a process that requires activation of the calcium-activated protease, calpain (Chen et al., 2007). Although fetal AChRs are permeable to $Ca^{2+}$, calpain remains activated well beyond the interval anticipated for AChR gating, suggesting that the $Ca^{2+}$ arises from another source (Chen et al., 2007). Because of the proximity of $IP_3R_1$ to the mature NMJ, we tested whether persistent calpain activation required release of $Ca^{2+}$ through $IP_3Rs$ in C2C12 cells expressing laminin-induced AChR clusters (Weston et al., 2007). First, we applied the small interference RNA technique to selectively knock down $IP_3R_1$, the most abundant $IP_3R_1$ in skeletal muscle (Wells, 2004). We compared the effect of six siRNA segments alone or in pairs (see Materials and Methods). We found that two segments, S1 and S2, together resulted in ~95% suppression of $IP_3R_1$ protein by day 3 after transfection of cultures (Fig. 1*A*, left) with marked reduction of $IP_3R_1$-specific immunofluorescence in C2C12 cells (Fig. 1*A*, right). In our hands the time course of calpain activation in C2C12 cells upon exposure to the cholinergic agonist, carbachol or CCh, was similar to that reported previously (Chen et al., 2007). Calpain levels remained constant in the absence of CCh but began to increase minutes after exposure, reaching a peak twice the basal level at 1 h (Fig. 1*B*). In the presence of 100 $\mu$M $Ca^{2+}$ added to the medium, the peak calpain reached 2.8 times over baseline during the same time course. The increase in calpain activity induced by CCh was completely blocked by either XS (xestospongin C) or 2-APB (2-aminoethoxydiphenyl borate), both blockers of the $IP_3$ receptor, without apparent effect on viability (Fig. 1*B*). siRNA knockdown of $IP_3R_1$ in C2C12 cells for 3 d caused a slight reduction in the basal activity of calpain without CCh treatment (Fig. 1*B*). siRNA-mediated $IP_3R_1$ knockdown had a nearly identical effect as 2-APB and XS in preventing CCh-induced calpain increases, while control RNA had no effect (Fig. 1*B*). This indicates that calpain elevation depends on the presence of intact, functioning $IP_3R_1$ in muscle cells.

Since calpain is implicated in AChR dispersal in myoblasts, we explored the role of $IP_3R_1$-derived $Ca^{2+}$ release in this early synaptic developmental event. C2C12 induced to form AChR clusters on laminin was incubated with CCh as described above. AChR clusters were enumerated at intervals up to 2 h after labeling with TxR-$\alpha$BT. As noted previously, exposure to CCh accelerates the rate of dispersal of AChR clusters in C2C12 beginning within 15 min, particularly in the presence of increased extracellular $Ca^{2+}$ (Fig. 1*C*) (Chen et al., 2007). However, when C2C12 were treated with either XS or 2-APB, AChR cluster dispersal was largely prevented (Fig. 1*C*). Furthermore, we show that $IP_3R_1$ silencing had

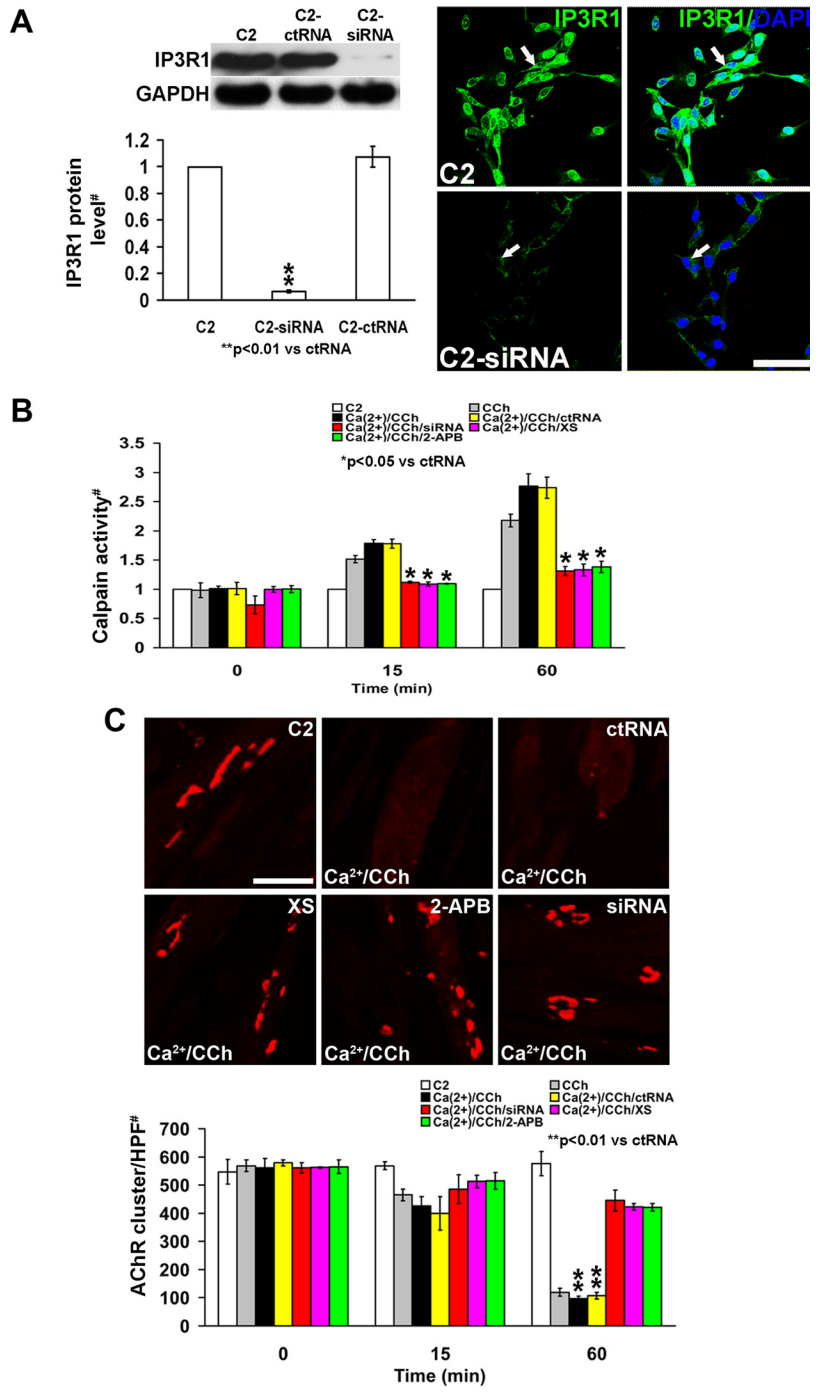


**Figure 1.** siRNA-mediated $IP_3R_1$ knockdown reduces calpain activity and stabilizes AChR clusters in C2C12 cells. ***A***, Left, Transfection of two $IP_3R_1$-specific siRNA sequences to C2C12 (C2-siRNA) significantly reduced $IP_3R_1$ protein level to 0.07 ± 0.01 of normal C2C12 (C2), while no difference was detected in control RNA-treated C2C12 (C2-ctRNA; 1.07 ± 0.08) (#, normalized to untreated C2). Right, C2C12 cells, treated as indicated in the panels and immunostained with antibody to $IP_3R_1$ (green), show marked reduction in $IP_3R_1$ immunostaining in C2C12 cells treated with $IP_3R_1$-specific siRNA compared to normal or ctRNA-treated C2C12; $n = 3$; $^{**}p < 0.01$, Student's *t* test. All other comparisons are not significant. ***B***, Time course of calpain activity (#, normalized to 0 time) in C2C12 cells treated with the following: media alone (C2); carbachol (CCh; 10 μM); C2/CCh with 100 μM calcium ($Ca^{2+}$/CCh); C2/$Ca^{2+}$/CCh after control RNA ($Ca^{2+}$/CCh/ctRNA); $Ca^{2+}$/CCh after siRNA-mediated $IP_3R_1$ knockdown ($Ca^{2+}$/CCh/siRNA); $Ca^{2+}$/CCh with 10 μM xestospongin ($Ca^{2+}$/CCh/XS); and $Ca^{2+}$/CCh with 50 μM 2-APB ($Ca^{2+}$/CCh/2-APB). After treatment for 60 min, calpain activity for CCh, $Ca^{2+}$/CCh, and $Ca^{2+}$/CCh/ctRNA was 2.18 ± 0.11, 2.77 ± 0.21, and 2.74 ± 0.18-fold over untreated C2, respectively. After pretreatment of C2 with siRNA-$IP_3R_1$, XS, and 2-APB, carbachol-induced calpain activity was 1.31 ± 0.79 ($Ca^{2+}$/CCh/siRNA), 1.33 ± 0.10 ($Ca^{2+}$/CCh/XS), and 1.38 ± 0.10 ($Ca^{2+}$/CCh/2-APB), respectively, significantly less than control not pretreated; $n = 3$, $^{*}p < 0.05$, Mann–Whitney *U* test. All other comparisons are not significant. ***C***, Top, AChR clusters expressed in untreated and treated C2C12 cultures. AChR clusters labeled with TxR-αBT were prominent in C2, $Ca^{2+}$/CCh/siRNA, $Ca^{2+}$/CCh/XS, and $Ca^{2+}$/CCh/2-APB and visibly reduced in CCh, $Ca^{2+}$/CCh, and $Ca^{2+}$/CCh/ctRNA, Scale bar, 40 μm. Bottom, AChR cluster density [#, high-powered field (HPF)] in cultures untreated (C2, 575.7 ± 42.7) and treated for 60 min with $Ca^{2+}$/CCh/siRNA (445.3 ± 37.2), $Ca^{2+}$/CCh/XS (422.7 ± 11.5), and $Ca^{2+}$/CCh/2-APB (420.3 ± 13.3) was significantly greater than in those treated with CCh (119.7 ± 13.5), $Ca^{2+}$/CCh (97.3 ± 7.8), and $Ca^{2+}$/CCh/ctRNA (107.3 ± 11.6); $n = 3$, $^{**}p < 0.01$, Student's *t* test. All other comparisons are not significant.

an equivalent effect on preventing AChR cluster dispersal as the drug treatment while control RNA had no effect, indicating a specificity for type 1 $IP_3R$ (Fig. 1*C*). Thus, agonist-induced AChR cluster dispersal, an early event in neuromuscular development, requires the participation of $IP_3R_1$, presumably for amplification of internal $Ca^{2+}$ levels and activation of cytosolic calpain.

### Muscle $IP_3R_1$ activity influences presynaptic and postsynaptic neuromuscular transmission and presynaptic vesicle recycling in NMJ

Many synapses exhibit the property of homeostatic plasticity, in which reductions in synaptic activity lead to compensatory increases in presynaptic strength, usually observed as an increase in transmitter release (Murthy et al., 2001). In the NMJ, partial blockade of neuromuscular activity by TTX or endplate AChRs by αBT for durations of 8–14 d changes the activity of the presynaptic neuron. TTX blockade leads to an increase in quantal size and probability of release, as well as increased postsynaptic ACh sensitivity. αBT blockade increases quantal content by increasing the number of releasable vesicles, suggesting that the NMJ is governed by tightly controlled homeostatic plasticity (Plomp et al., 1992; Wang et al., 2010). We hypothesized that the effect of cholinergic input in eliciting homeostatic plasticity is mediated through the skeletal muscle $IP_3R_1$ receptor. We reasoned that systemic pharmacologic blockade of $IP_3Rs$ was likely to have nonspecific effects in an electrophysiological study. Therefore, we set up a system for subacute silencing of $IP_3R_1$ *in vivo* by directly electroporating $IP_3R_1$-specific siRNA into TA muscle (Golzio et al., 2005). Preliminary experiments using a GFP reporter plasmid and siRNA specific for the GFP showed that this procedure achieved expression of GFP in 80–90% of muscle fibers (Fig. 2*A*), and siRNA specific for GFP reduced levels of overexpressed GFP activity to 16% of control after 5 d (Fig. 2*A*). For *in vivo* silencing of $IP_3R_1$, we employed the same siRNA sequences applied for the C2C12 cells. We found that the $IP_3R_1$ levels were decreased to ≤15% of the level

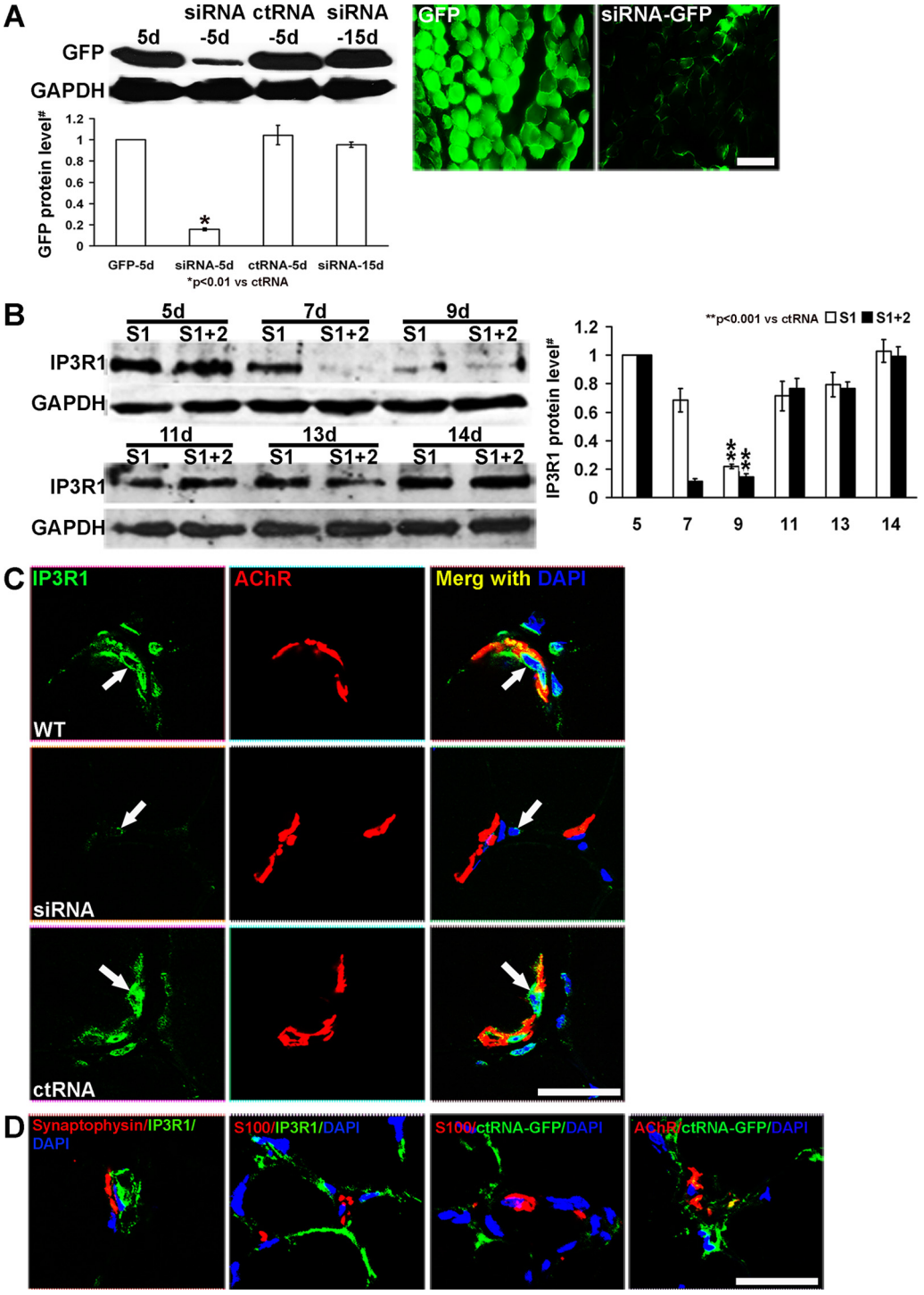


**Figure 2.** Reduced expression $IP_3R_1$ in tibialis anterior and neuromuscular junction by siRNA-mediated $IP_3R_1$ knockdown. ***A***, Left, Transfection TA muscle with GFP-specific siRNA sequence and GFP plasmid significantly reduced GFP protein level to 0.16 ± 0.01 of GFP-electroporated TA muscle on day 5, while no difference was detected in control RNA-treated, GFP-transfected TA muscle (ctRNA-5 d; 1.04 ± 0.09). Fifteen days after electroporation of TA with GFP-siRNA and GFP plasmid (siRNA,15 d), GFP protein level returned to 0.95 ± 0.03 of GFP-plasmid transfected TA (#, normalized to only GFP-expressed TA muscle on days 5). Right, TA muscle treated as indicated in panels and compared to normal GFP-expressed TA muscle. GFP fluorescence showed remarkable reduction in TA muscle treated with GFP-specific siRNA; $n = 3$; $^*p < 0.01$, Student's $t$ test. All other comparisons are not significant. ***B***, Electroporation of two $IP_3R_1$-specific siRNA sequences (S1 and S2) into TA muscle diminished $IP_3R_1$ expression maximally between days 7 and 9. $IP_3R_1$ protein level (#, normalized to untreated) was reduced to 0.11 ± 0.02 and 0.15 ± 0.02% of untreated on days 7 and 9, respectively, and recovered 0.99 ± 0.06% on day 14; $n = 9$, $^{**}p < 0.001$, Mann–Whitney $U$ test. All other comparisons are not significant. ***C***, $IP_3R_1$ immunostained with antibody to $IP_3R_1$ (green) colocalizes with NMJ labeled with TxR-$\alpha$BT (red) and surrounded by subsynaptic DAPI-labeled nuclei (blue) in WT and ctRNA-treated normal TA muscle. Expression of $IP_3R_1$ at NMJ was nearly eliminated in all nine TA muscles electroporated with $IP_3R_1$ siRNA. Scale bar, 12 $\mu$m. ***D***, Immunostaining of $IP_3R_1$ (green) does not colocalize with synaptophysin (red), a subsarcolemmal region, and does not colocalize with S100 protein (red, middle right panel), When labeled for AChRs with TxR-$\alpha$BT, muscle electroporated with GFP-ctRNA shows the RNA in the subsarcolemmal region surrounding the TxR-$\alpha$BT-labeled endplates (red, far right panel). Scale bar, 12 $\mu$m.

seen in untreated TA between days 7–9 postelectroporation and returned to normal levels at day 14 after electroporation of $IP_3R_1$-specific siRNAs (Fig. 2*B*). Immunostaining for $IP_3R$ showed that $IP_3R_1$ silencing had a pronounced effect on $IP_3R$ expression at NMJs. NMJs in both untreated and control RNA-treated muscles had intense labeling of $IP_3Rs$ colocalized with AChRs and subsynaptic nuclei (Fig. 2*C*), while NMJs in siRNA-treated muscle had greatly reduced immunostaining of $IP_3Rs$ at both AChRs and subsynaptic nuclei. Figure 2*D* shows that $IP_3R$ silencing by siRNA electroporation was specific for muscle and NMJ. Compared with Figure 4*C*, $IP_3R_1$ did not colocalize with nerve termini labeled for synaptophysin (Fig. 2*D*, far left panel) or Schwann cell nuclei labeled with S100 (Fig. 2D, middle left panel). We also used GFP-labeled control siRNA to demonstrate the distribution of electroporated RNA in muscle. We found that siRNA was mainly located in the subsarcolemmal region, including NMJs, whereas no siRNA colocalized with Schwann cells marked by S100 protein (Fig. 2*D*, middle right panel) but did overlap with the endplate regions (Fig. 2*D*, far right panel). Silencing of $IP_3R_1$ had no effect on levels of expression of other muscle proteins, such as RyR1 and L-type calcium channel alpha 1 subunit, at 9 d (data not shown).

We studied the effect of $IP_3R_1$ knockdown on neuromuscular transmission in TA muscle pretreated 9 d earlier with $IP_3R_1$-siRNA by using the two-electrode voltage-clamp technique. We recorded both spontaneous MEPCs (miniature endplate currents) and EPCs (endplate currents) evoked by direct stimulation of the attached sciatic nerve and characterized both the presynaptic and postsynaptic components of neuromuscular transmission (Ikeda et al., 1984). Figure 3*A* (left) shows raw data tracings of spontaneous activity for TA muscle treated 9 d previously with ctRNA (scrambled RNA) or $IP_3R_1$-siRNA.

Figure 3, *B* and *C*, shows that both the amplitude ($3.86 \pm 0.32$ nA vs $2.53 \pm 0.29$ nA, $p < 0.05$) and decay phase of MEPCs ($1.5 \pm 0.08$ ms vs $1.14 \pm 0.15$ ms, $p < 0.05$) were significantly increased in TA muscle treated with siRNA-$IP_3R_1$ (by 52 and 31%, respectively), relative to contralateral control-treated TA. MEPC parameters in control-treated TA were no different from untreated muscle. These findings indicate that $IP_3R_1$ plays an important role in modulating the postsynaptic component of neuromuscular transmission. In addition, the frequency of MEPCs ($3.11 \pm 0.26\ s^{-1}$ vs $1.4 \pm 0.09\ s^{-1}$, $p < 0.001$; Fig. 3*A*, right) more than doubled, suggesting that $IP_3R_1$ has an additional role in modulating the presynaptic component of transmission, i.e., on release of neurotransmitter from the presynaptic sites. These combined presynaptic and postsynaptic changes were accompanied by an ~2-fold increase in the amplitude of the EPC (endplate current) evoked by sciatic nerve stimulation ($122.49 \pm 12.92$ vs $50.21 \pm 5.9$ nA, $p < 0.001$; Fig. 3*D*). Finally, the quantal content ($34.2 \pm 1.8$ vs $26.08 \pm 3.96$, $p < 0.05$) increased by 30% (Fig. 3*E*). These observations are similar to those seen in the TTX and $\alpha$BT partial blockade models and suggest that $IP_3R_1$-mediated $Ca^{2+}$ release from internal stores in muscle at the NMJ mediates the action of cholinergic input on both presynaptic and postsynaptic aspects of homeostatic plasticity (Wang et al., 2005, 2010).

### $IP_3R_1$ activity controls synaptic gene expression in muscle

The increase in amplitudes and decay phases of MEPCs induced by $IP_3R_1$ silencing suggests that $IP_3R_1$ signaling is involved in AChR expression. To test this, we first compared AChR expression by measuring fluorescence intensity of endplates labeled with TxR-$\alpha$BT in muscle treated by denervation, which is known to increase AChR expression, or by siRNA $IP_3R_1$ knockdown. We found that $IP_3R_1$ knockdown in TA muscle was associated with a 1.8-fold increase in endplate AChR intensity, a smaller, but similar effect on AChR expression as that seen with denervation (Tsay and Schmidt, 1989; Akaaboune et al., 1999) (Fig. 4*A*). The change in AChR expression is in good agreement with the 1.5-fold increase in MEPC amplitudes induced by $IP_3R_1$ silencing (Fig. 3*B*).

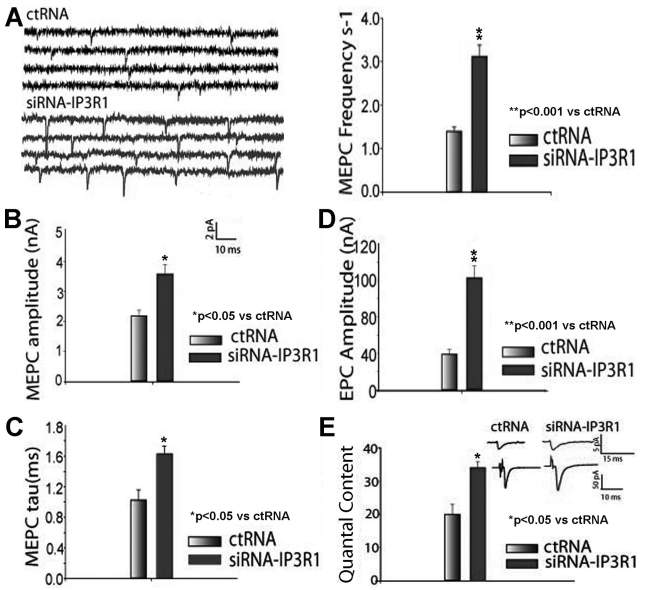


**Figure 3.** siRNA-mediated $IP_3R_1$ silencing alters presynaptic and postsynaptic components of neuromuscular transmission. ***A***. Left, Representative traces of MEPCs in ctRNA-treated (top, black) and $IP_3R_1$-siRNA-treated (bottom, blue) normal tibialis anterior muscle voltage clamped at −60 mV. Right, The frequency of spontaneous MEPC was significantly increased in $IP_3R_1$-siRNA-treated muscle compared with ctRNA-treated TA ($n = 29$) ($3.11 \pm 0.26\ s^{-1}$; $n = 49$ vs $1.4 \pm 0.09\ s^{-1}$; $n = 29$, $^{**}p < 0.001$). ***B***, MEPC amplitudes from $IP_3R_1$-siRNA-treated TA muscle ($3.86 \pm 0.32$ nA; $n = 25$) were nearly 2-fold greater than those recorded from ctRNA-treated TA muscle ($2.53 \pm 0.29$ nA; $n = 19$, $^{*}p < 0.05$). ***C***, The MEPC ($\tau$) in $IP_3R_1$-siRNA-treated TA muscle ($1.5 \pm 0.08$ ms; $n = 25$) was significantly increased compared with that of ctRNA ($1.14 \pm 0.15$ ms; $n = 19$, $^{*}p < 0.05$). ***D***, EPC amplitude of $IP_3R_1$-siRNA-treated TA muscle was significant greater than that of the ctRNA-treated muscle ($50.21 \pm 5.9$ nA; $n = 26$ vs $13.72 \pm 2.8$ nA; $^{**}p < 0.001$, $n = 26$). ***E***, The quantal content of evoked transmitter release was significantly increased in $IP_3R_1$-siRNA-treated TA muscle compared with ctRNA-treated muscle ($34.2 \pm 1.8$ vs $26.08 \pm 3.96$, $^{*}p < 0.05$) and increased by 30% ($n = 26$). Inset shows raw data trace of EPC for $IP_3R_1$-siRNA-treated and ctRNA-treated muscle; $n = \#$ of endplates. Mouse $\# = 10$. All comparisons were analyzed by Student's *t* test. All other comparisons are not significant.

Since cholinergic input influences both synaptic currents and contractile (electrical) activity, it is difficult to separate the differential effects of these two variables and their modes of coupling to gene expression. Studies have pointed to a role for the L-type $Ca^{2+}$ channel as the principal intracellular $Ca^{2+}$ source for signals coupled to electrical activity (Friedrich et al., 2008). Based on the striking colocalization of $IP_3R_1$ with AChRs and subsynaptic nuclei at the NMJ, we hypothesized that this channel is a source of internal $Ca^{2+}$ involved in regulating synaptic muscle gene expression. We studied the effect of $IP_3R_1$ silencing on expression of a panel of NMJ and muscle-specific genes. We first investigated the time course of AChR gene expression between 3 and 14 d after knockdown, an interval that spans the duration of the effect of a single siRNA electroporation on $IP_3R_1$ expression, and then used quantitative RT-PCR to compare this effect to that of denervation.

In siRNA-treated muscle, expression levels of both $\alpha$ and $\gamma$ subunit genes began to increase steadily 3 d after siRNA knockdown until reaching peak levels of >10-fold and >60-

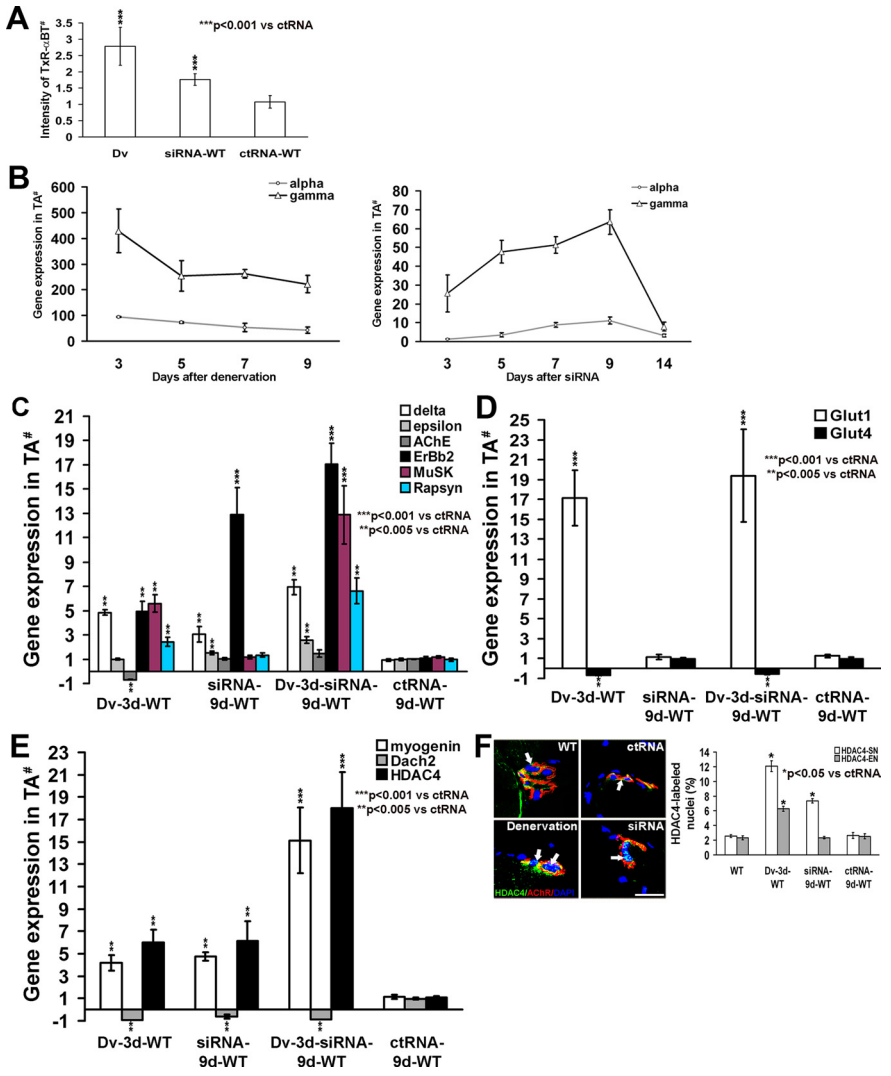


**Figure 4.** $IP_3R_1$ activity controls synaptic gene expression in muscle. ***A***, AChR intensity (TxR-αBT fluorescence intensity; #, normalized to untreated) at WT NMJ after treatment with siRNA (siRNA-WT) for $IP_3R_1$ knockdown (9 d) is 1.76 ± 0.18-fold greater than untreated, a significant increase compared with untreated ($n = 7$; $^{***}p < 0.001$), while ctRNA (ctRNA-WT) had no effect ($n = 7$; $p > 0.81$). After denervation (Dv), the AChR intensity was increased by 2.79 ± 0.58-fold, significantly greater than untreated ($n = 7$; $^{***}p < 0.001$). ***B***, Time course of expression (#, normalized to 0 time expression) of α and γ subunit after denervation (left graph), or after siRNA silencing of $IP_3R_1$ (right graph). Expression levels at day 9 after siRNA for α subunit (11.12 ± 1.83) and γ subunit (63.48 ± 6.49) were significantly greater than the corresponding values for ctRNA-treated TA muscle ($n = 5$; $p < 0.005$). ***C***, Expression levels (#, normalized to 0 time expression) of NMJ genes, AChR δ subunit (delta), AChR ε subunit (ε), acetylcholinesterase (AChE), ErbB2, MuSK, and rapsyn in TA muscle. Expression levels at day 9 after siRNA for δ subunit (3.07 ± 0.64; $^{**}p < 0.005$) and ε subunit (1.52 ± 0.16; $^{**}p < 0.005$) were significantly greater than the corresponding values for ctRNA-treated TA muscle ($n = 5$). Treatment with denervation for 3 d (DV-3d-WT), $IP_3R_1$ knockdown for 9 d (siRNA-9d-WT), combined denervation and $IP_3R_1$ knockdown (DV-3d-siRNA-9d-WT), or ctRNA for 9 d (ctRNA-WT) showed similar but not identical effects of the two treatments on gene expression. Combined treatments showed that effects are overlapping. $^{***}p <$ 0.001. ***D***, Expression levels (#, normalized to 0 time expression) of muscle genes, Glut1 and Glut4, in TA muscle after treatment with denervation for 3 d (DV-3d-WT), $IP_3R_1$ knockdown for 9 d (siRNA-9d-WT), combined denervation and $IP_3R_1$ knockdown (DV-3d-siRNA-9d-WT), or ctRNA for 9 d (ctRNA-WT) showed that $IP_3R_1$ had no effect on non NMJ muscle gene expression compared with denervation. Compared to WT, expression of Glut1/4 was unchanged in siRNA-9d-WT and ctRNA-9d-WT, whereas Glut1 expression was >15-fold to WT in Dv-3d-siRNA-9d-WT and in Dv-3d-WT. ctRNA had no effect on gene expression; $n = 5$; $^{**}p < 0.005$, $^{***}p < 0.001$. ***E***, Expression levels (#, normalized to 0 time expression) of regulatory genes, myogenin, Dach2, and HCAC4 in TA muscle after treatment with denervation for 3 d (DV-3d-WT), $IP_3R_1$ knockdown for 9 d (siRNA-9d-WT), combined denervation and $IP_3R_1$ knockdown (DV-3d-siRNA-9d-WT), or ctRNA for 9 d (ctRNA-WT) demonstrated that comparable effects on regulatory genes was significantly increased by $IP_3R_1$ knockdown and denervation. ctRNA had no effect on gene expression; $n = 5$; $^{**}p < 0.005$, $^{***}p < 0.001$. ***F***, Left, Immunolocalization of HDAC4 in subsynaptic nuclei of wild-type (WT), denervated (Dv), siRNA-treated (siRNA), and control RNA-treated (ctRNA) TA muscle colabeled with TxR-αBT (red) and DAPI (blue) to label nuclei shows that HDAC4 (green) is localized at and surrounding NMJs in all four panels, but in addition shows colocalization with subsynaptic nuclei (light blue stain) in denervated and siRNA-treated TA muscle (arrows). Scale bar, 15 μm. Right, Quantification of HDAC4 immunolabeling in subsynaptic nuclei (SN) and extrajunctional nuclei (EN) showed that the percentage of HDAC4-labeled subsynaptic nuclei (HDAC4-SN) in denervated TA muscle (Dv-3d-WT) and siRNA-9d-WT were 12.07 ± 0.73 and 7.36 ± 0.29%, respectively, both significantly greater than WT (2.56 ± 0.21%) and ctRNA-9d-WT (2.04 ± 0.41%) ($n = 3$; $^{*}p < 0.05$). The percentage of HDAC4-labeled extrajunctional nuclei (HDAC4-EN) in Dv-3d-WT 6.27 ± 0.35% was significantly greater than those found in WT (2.34 ± 0.28%), siRNA-9d-WT (2.33 ± 0.16%), and ctRNA-9d-WT (2.51 ± 0.34%); $n = 3$; $^{*}p <$ 0.05. All comparisons were analyzed by Mann–Whitney *U* test. All other comparisons not significant.

fold over baseline, respectively, after 9 d (Fig. 4*B*, right). The sharp peak and decline in AChR gene expression after $IP_3R_1$ knockdown in muscle were coincident with the time course of $IP_3R_1$ silencing (Fig. 2*B*). The increase in δ gene expression was more modest, peaking at day 9 (Fig. 4*C*). $IP_3R_1$ had a small but significant effect on ε subunit expression over the same time course as the δ subunit (Fig. 4*C*). Control RNA had no effect on AChR subunit gene expression. In contrast, as reported previously, after denervation α, γ, and δ subunit expression increased immediately after 3 d and remained significantly elevated for at least 9 d (Tsay and Schmidt, 1989; Akaaboune et al., 1999) (Fig. 4*B*, left and right). The increases after denervation were of greater magnitude, but the differential effects on α, γ, and δ subunit expression were comparable. However, as reported previously, denervation had little effect on ε subunit expression, particularly at day 3, when expression of the other subunits increases (Fig. 4*C*) (Martinou and Merlie, 1991). The increases in AChR subunit gene expression, including the appearance of the (embryonic) γ subunit expression (slower channel kinetics), are consistent with the finding that $IP_3R_1$ knockdown increased MEPC amplitudes and MEPC decay phase duration (Fig. 3*B*,*C*). These studies suggest that the effect of $IP_3R_1$ may resemble the effect of denervation on AChR gene expression, although differences in the control of ε subunit expression may point to distinct influences on synaptic genes.

To test whether $IP_3R_1$ silencing influences a wider array of NMJ and muscle-specific genes similar to the role of cholinergic input, we compared the effect of muscle $IP_3R_1$ silencing (day 9) with the effect of denervation (day 3) on the expression of a panel of other muscle-specific genes known to be influenced by cholinergic activity. Figure 4*C* showed that, like denervation, $IP_3R_1$ silencing led to increased expression of rapsyn and the neuregulin receptor ErbB2. Curiously, as with the AChR genes, the effect of $IP_3R_1$ silencing on rapsyn was of smaller magnitude than

←

denervation, but the effect of $IP_3R_1$ silencing on ErbB2 expression was >2-fold that of denervation. Moreover, $IP_3R_1$ silencing did not alter muscle-specific receptor tyrosine kinase (MuSK) or acetylcholinesterase (AChE) expression, while denervation increased MuSK and decreases AChE expression. For more widely expressed genes, $IP_3R_1$ silencing had no effect on extrajunctional muscle genes such as the glucose transporters glut1 and glut4, while denervation increased expression of glut1 and decreased expression of glut4 (Fig. 4*D*) (Jones et al., 1998). These findings indicate that $IP_3R_1$ activity has a distinct influence on the expression of synapse-specific genes.

Modulation of some NMJ-localized genes and other extrajunctional muscle genes by denervation, but not by $IP_3R_1$ silencing, is in agreement with observations that expression of these genes is under control of multiple factors, including electrical activity, and peptide modulators such as neuregulin and agrin (Lømo et al., 1985; Goldman et al., 1988; Tsay and Schmidt, 1989; Yang et al., 1991; Castelló et al., 1993; Jones et al., 1998; Moore et al., 2001; Lebrasseur et al., 2003). The fact that $IP_3R_1$ silencing, which leaves muscle innervation and contraction intact, also increases expression of some NMJ genes, particularly ErbB2, and selectively increases expression of the ε subunit, suggests that there are additional overlapping factors that influence synaptic gene expression (Lebrasseur et al., 2003; Sunesen and Changeux, 2003). Therefore, we explored the effect of combined $IP_3R_1$ silencing and denervation. Nine days before harvesting muscle, the TA was electroporated with siRNA for $IP_3R_1$ or control RNA. Three days before harvest, TA muscles were denervated. Figure 4, *C* and *D*, compares the effect of denervation alone, of $IP_3R_1$ silencing alone and of denervation following $IP_3R_1$ silencing for 9 d on muscle gene expression. $IP_3R_1$ silencing had no greater effect on expression of glut1 and glut4 even when combined with denervation. However, we found that expression of both the δ subunit and rapsyn, which were increased by $IP_3R_1$ silencing alone, were further increased by denervation, greater than by denervation alone. In addition, while $IP_3R_1$ silencing had no effect on expression of MuSK or AChE, the combined effect of $IP_3R_1$ silencing and denervation significantly increased MuSK expression and eliminated the effect of denervation on AChE expression. More importantly, while the effect of $IP_3R_1$ silencing was to increase expression of ε subunit and that of ErbB2 greater than the effect of denervation, the combined effect of siRNA and denervation was significantly greater than the effect of $IP_3R_1$ silencing or denervation alone. One interpretation of these findings is that $IP_3R_1$ activity, and presumably synaptic $Ca^{2+}$ fluxes, exert distinct localized control on NMJ gene expression.

To investigate whether overlapping influences on muscle gene expression between cholinergic input and $IP_3R_1$ activity can be explained by changes in transcription or protein expression, we studied the expression of the HLH (helix-loop-helix) family of transcription factors involved in muscle gene expression. We found that both denervation and $IP_3R_1$ silencing led to increases in myogenin and HDAC4 and reduced expression of Dach-2 within muscle fibers (Fig. 4*E*), suggesting that both treatments equally influenced expression of these transcription factors at the gene level. These findings are consistent with the observation that many downstream muscle genes are influenced by both denervation and $IP_3R_1$ silencing. We also detected expression of this panel of genes in muscle with 2-APB-mediated blockade of $IP_3R$ and selective elimination of muscle IP3 by INPP5a, and the results were similar as with $IP_3R_1$ silencing (data not shown).

Changes in skeletal muscle gene expression mediated by muscle electrical activity and $Ca^{2+}$ fluxes are partly regulated by the CaMKII-dependent nucleocytoplasmic shifts of the transcription protein HDAC4 and direct binding and reciprocal regulation of MEF2 transcription factor activity (Tang et al., 2004; Cohen et al., 2007). Because $IP_3R_1$ mediates localized $Ca^{2+}$ fluxes at the NMJ that can activate CaMKII and phosphorylate HDAC4, we compared the effect of denervation, known to increase myonuclear translocation of HDAC4, with the effect of siRNA silencing of $IP_3R_1$ *in vivo* on myonuclear translocation of HDAC4. Denervation of TA muscle was associated with a 3-fold increase in the proportion of extrajunctional myonuclei labeling for HDAC4, from 2.34 ± 0.3% in innervated muscle to 7.46 ± 0.3% after denervation (HDAC-EN; Fig. 4*F*; $n = 3$, $p < 0.05$). Looking specifically at subsynaptic nuclei in TA muscle fibers, we found that denervation caused a 4-fold shift in the number of HDAC4-positive subsynaptic nuclei (10.88 ± 0.8%, HDAC4-SN; $n = 3$, $p < 0.05$) compared with innervated TA muscle (2.56 ± 0.2%; Fig. 4*F*). In comparison, siRNA-$IP_3R_1$ treatment of TA muscle caused a nearly 3-fold increase (7.36 ± 0.3%; $n = 3$, $p < 0.05$) in HDAC4-positive subsynaptic nuclei but had no effect on HDAC-positive extrajunctional nuclei (2.33 ± 0.2%, HDAC4-EN; Fig. 4F; $n = 3$, $p > 0.87$). Control RNA had no effect on HDAC4 labeling of TA muscle nuclei in either compartment (Fig. 4*F*). The changes in NMJ nuclear expression of HDAC4 are highly consistent with the selective changes in NMJ gene expression and suggest that $Ca^{2+}$ released through $IP_3R_1$ at the NMJ acts via synaptic myonuclear HDAC4 to regulate NMJ-specific gene expression. The results point to a role for $IP_3R_1$ in targeting the synaptic effects of cholinergic input to mediate localized gene expression through an HDAC4 mechanism.

### $IP_3R_1$ silencing prevents pathological $Ca^{2+}$ overload, cysteine protease activation, and degeneration of NMJs

Numerous pathological processes, such as seizure activity, excitotoxicity, organophosphorus poisoning, or excessive anticholinesterase medication, lead to deleterious increases in cytoplasmic $Ca^{2+}$, synaptic degeneration, and neuronal death (Ariens et al., 1968; Choi, 1992, 1995; Kobayashi et al., 2009; Thiermann et al., 2009). Agonist myopathy is an acute model of cholinergic excitotoxicity induced by excessive inhibition of anticholinesterases as used in therapy for myasthenia gravis (Leonard and Salpeter, 1979; Kawabuchi, 1982). It is associated with pathological accumulation of $Ca^{2+}$ and degeneration of the NMJ. SCS is a genetic disorder in which mutations in the AChR cause prolonged AChR gating and overload of the NMJ with $Ca^{2+}$, resulting in degeneration of the NMJ (Engel et al., 1996; Gomez et al., 1997, 1998). In a mouse model for SCS in which the clinical, pathological, and electrophysiological features of the disease are reproduced by muscle expression of the AChR subunit bearing SCS mutations such as εL269F, fura-2 imaging studies suggested that $Ca^{2+}$ overload in this disorder depends on IP3 receptor-gated stores rather than $Ca^{2+}$ entry through L-type channels or ryanodine receptors (Gomez et al., 1997; Zayas et al., 2007).

We hypothesized that $IP_3R$ blockade or selective reduction of $IP_3R_1$ by siRNA knockdown *in vivo* would prevent pathological accumulation of postsynaptic $Ca^{2+}$ at the NMJ. TA muscles of wild-type (WT) mice were pretreated by electroporation with siRNA-$IP_3R_1$ or control RNA in contralateral hind limbs. Nine days later mice were injected intraperitoneally with the cholinesterase inhibitor neostigmine (0.25 mg/kg), a dose previously established to cause NMJ $Ca^{2+}$ overload based on the GBHA histochemical stain and degeneration of NMJ (Leonard and Salpeter, 1979; Kawabuchi, 1982). After 36 h, endplate $Ca^{2+}$ deposits were identified at ~39.8 ± 4.5% of endplates in nonpretreated

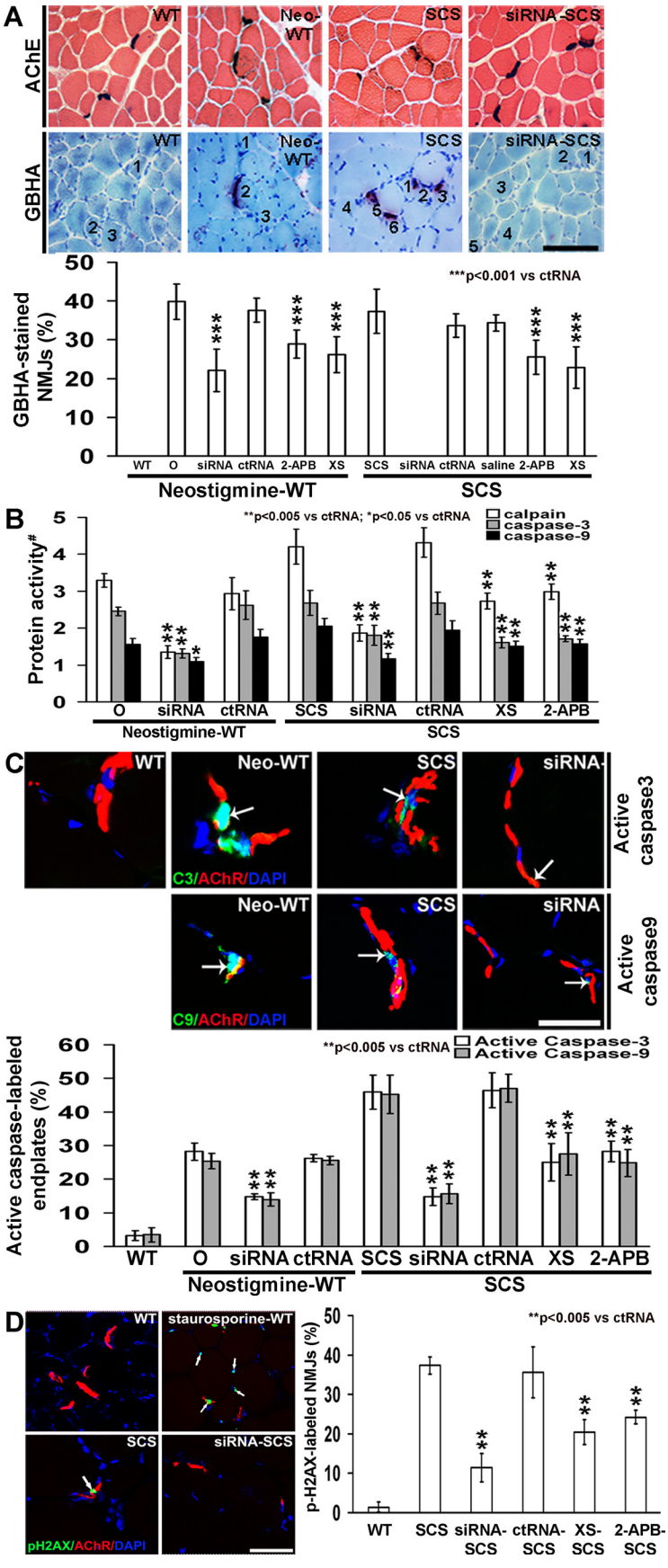


**Figure 5.** $IP_3R_1$ activity is required for $Ca^{2+}$ overload of NMJs and pathological activation of calpain, caspase-3, and caspase-9 at NMJs. ***A***, Top, Serial TA muscle sections labeled for cholinesterase (dark brown) to localize endplates and GBHA (red) to localize $Ca^{2+}$ overloading in WT, SCS, WT pretreated with excessive dose of neostigmine (Neo-WT), and SCS muscle after $IP_3R_1$-siRNA (*Figure legend continues.*)

mice, which was reduced to 22.1 ± 5.5% in mice pretreated with siRNA-$IP_3R_1$ (Fig. 5*A*; $n = 7$, $p < 0.001$). Control RNA had no effect on neostigmine-induced NMJ $Ca^{2+}$ overload (37.6 ± 3.1%; Fig. 5*A*). Blockade of $IP_3$ receptors by systemic pretreatment of mice for 9 d with the nonspecific blocker 2-APB or XS also reduced the proportion of GBHA-labeled endplates to 28.9 ± 3.6% and 26.2 ± 4.6%, respectively (Fig. 5A; $n = 7$, $p < 0.001$).

Muscle from both SCS patients and SCS transgenic mice bearing different AChR mutations have $Ca^{2+}$-overloaded NMJs proportional to the severity of the effect of the mutation on the prolongation of synaptic currents (Gomez et al., 1997, 2002; Zayas et al., 2007). In this study we employed the SCS mouse line expressing εL269F, which has the most extensive endplate $Ca^{2+}$-overload of a series of five lines studied in detail (Gomez et al., 1997, 2002; Zayas et al., 2007). We found that electroporation of siRNA-$IP_3R_1$ into TA muscle of SCS mice completely eliminated the $Ca^{2+}$ overload of NMJs at 9 d (Fig. 5*A*; $n = 7$), while control RNA had no effect (33.4 ± 3.1%; Fig. 5*A*; $n = 7$, $p > 0.91$). Also, treatment of SCS mice with the $IP_3R$ blocker 2-APB or XS for 2 d significantly reduced the proportion of GBHA-labeled endplates to 25.5 ± 4.4 and 22.9 ± 5.3%, respectively (Fig. 5A; $n = 7$, $p < 0.001$). These findings suggest that pathological elevation of $Ca^{2+}$ at the intact neuromuscular synapse *in vivo* requires participation of $IP_3R_1$-mediated $Ca^{2+}$ release in skeletal muscle.

Previous studies have shown that $Ca^{2+}$ overload in NMJs leads to activation of the $Ca^{2+}$-activated protease calpain and, indirectly, that of the caspase proteases caspase-3 and caspase-9, which contribute to NMJ degeneration (Leonard and Salpeter, 1979; Vohra et al., 2004, 2006). We found that genetic inhibition of calpain improved endplate ultrastructure, neuromuscular transmission, and muscle strength in SCS mice, but also found evidence for a significant role for caspases (Vohra et al., 2004, 2006; Groshong et al., 2007). Since siRNA-$IP_3R_1$ reduced or eliminated $Ca^{2+}$ accumulation at endplates with either Neostigmine treatment or in SCS, we tested whether $IP_3R_1$ silencing would prevent increases in calpain activity in neostigmine-treated WT mice and SCS transgenic mice. To measure calpain activity in muscle homogenates, we used a highly sensitive luciferase-based calpain assay that employs a luminogenic calpain substrate (Calpain-Glo, Promega). Calpain activity in both neostigmine-treated WT and SCS

mouse TA muscle was 3.3–4.2 times the level in untreated WT muscle (Fig. 5*B*). siRNA knockdown of $IP_3R_1$ in TA muscles 9 d before neostigmine treatment or in SCS TA muscles significantly reduced calpain activity to 1.4–1.9-fold of WT (Fig. 5*B*; $n = 7$, $p < 0.005$). Furthermore, treatment of SCS mice with $IP_3R$ inhibitors 2-APB ($n = 7$, $p < 0.005$) or XS ($n = 7$, $p < 0.005$) significantly reduced muscle calpain activity in SCS mice, although levels still remained 3.0- and 2.7-fold greater than WT, respectively (Fig. 5B).

Caspase activation at the NMJ of SCS patients presumably occurs via the intrinsic pathway when $Ca^{2+}$ overload provokes mitochondrial stress and release of cytochrome *c* (Boehning et al., 2003). Activated forms of caspases are detected at NMJs of SCS patients and SCS transgenic mice (Vohra et al., 2004). Using antibodies specific for activated caspases, the proportions of active caspase-labeled endplates are roughly equivalent to the proportions of $Ca^{2+}$-overloaded endplates in these mice. In mice treated with neostigmine 36 h before detection, >25% of endplates were labeled intensely for active caspase-9 and active caspase-3 (Fig. 5*C*). In εL269F SCS mice, ~45% of endplates were labeled with active caspase-9 and active caspase-3, as reported previously (Fig. 5*C*) (Vohra et al., 2004; Groshong et al., 2007).

Caspase activity can also be characterized using a luciferase-based luminogenic caspase substrate assay (Caspase-Glo 9 and Caspase-Glo 3/7, Promega) to study TA muscle homogenates. Caspase-9 activity in neostigmine-treated WT mice was 1.6-fold over the untreated level and was 2-fold over normal levels in SCS mouse TA muscle ($n = 5$, $p < 0.005$). Caspase-3 activity was 2.5-fold over the untreated levels in both neostigmine-treated WT and SCS mice (Fig. 5*B*; $n = 5$, $p < 0.005$).

Treatment of TA muscle with siRNA-$IP_3R_1$ by direct electroporation *in vivo* before neostigmine treatment significantly reduced the fraction of endplates labeled with activated caspase-9 and caspase-3 to 14 and 15% (Fig. 5*C*; $n = 5$, $p < 0.005$), respectively. Silencing of $IP_3R_1$ also completely prevented the increase in both caspase activities induced by neostigmine treatment, while control RNA had no effect. In SCS mice $IP_3R_1$ knockdown reduced the proportion of active caspase-9 and caspase-3-positive endplates >2-fold (Fig. 5*C*; $n = 5$, $p < 0.005$). Similarly, siRNA-$IP_3R_1$-treated SCS mice significantly decreased the activity of both caspases (Fig. 5*B*; $n = 5$, $p < 0.005$), whereas control RNA treatment had no effect in preventing caspase accumulation at endplates. Lastly, treatment of SCS mice with a nonspecific $IP_3R$ inhibitor, either 2-APB or XS, 2 d prior significantly diminished the accumulation of caspase-9 and caspase-3 (Fig. 5*C*; $n = 5$, $p < 0.005$) and diminished caspase-3 and caspase-9 activity (Fig. 5*B*; $n = 5$, $p < 0.005$, $p < 0.05$) at endplates. These findings demonstrate that in two models of synaptic $Ca^{2+}$ overload in muscle, acute pharmacological inhibition of acetylcholinesterase and the SCS mouse model, elevated caspase-3 and caspase-9 activity and accumulation of activated caspase-3 and caspase-9 at NMJs depend on the presence of skeletal muscle $IP_3R_1$, which presumably amplifies internal release of $Ca^{2+}$. Thus, in addition to its physiological role, $IP_3R_1$ plays a key role in pathological elevations of proteases at synapses.

NMJ regions of SCS mouse muscle fibers have evidence of DNA damage best seen by immunostaining for phosphorylated H2AX (pH2AX) at Ser139, a histone modification that initiates DNA damage repair (Rogakou et al., 2000) (Fig. 5*D*). Figure 5*D* shows that immunolabeling of pH2AX was seen selectively in subsynaptic nuclei of SCS mice labeling ~37% of NMJs, similar to the numbers seen for GBHA and active caspase labeling and as compared with extensive pH2AX labeling detected in widespread apoptosis-induced staurosporine treatment (Belmokhtar et al., 2001). $IP_3R_1$ knockdown significantly reduced the proportion of pH2AX-labeled NMJs to 11.4 ± 3.6% in SCS TA muscle (Fig. 5*D*; $n = 5$, $p < 0.005$). Control RNA did not reduce pH2AX-labeled endplates (35.6 ± 6.5%; $n = 5$; $p > 0.96$). Treatment of mice with

←

(*Figure legend continued.*) treatment (siRNA-SCS). $Ca^{2+}$ overloading was found at endplates of SCS transgenic mice (SCS) and neostigmine-treated wild type mice (Neo-WT), but not in wild type (WT) or siRNA-treated SCS mice (siRNA-SCS). Numbers on GBHA-labeled section corresponds to fibers with cholinesterase-stained endplates in adjacent section above. Scale bar, 60 μm. Bottom, Quantitation of $Ca^{2+}$ overload of endplates (percentage GBHA-labeled endplates) in neostigmine-treated WT and in untreated SCS mice and its dependence on $IP_3R_1$ activity. Endplates from WT TA showed no $Ca^{2+}$-labeled endplates, while a significant number of NMJs were overloaded with $Ca^{2+}$ after neostigmine treatment of WT mice (39.84 ± 4.54) or in untreated SCS (37.33 ± 5.7). siRNA treatment of TA muscle for $IP_3R_1$ knockdown significantly reduced $Ca^{2+}$ overload of endplates in neostigmine-treated mice (22.10 ± 5.46%) and abolished $Ca^{2+}$-overload of SCS endplates. ctRNA had no effect on neostigmine-induced endplate $Ca^{2+}$ overload (37.63 ± 3.06%) or $Ca^{2+}$ overload in SCS muscle (33.65 ± 3.07%). The nonspecific $IP_3R$ blocker 2-aminoethoxydiphenyl (2-APB), significantly reduced $Ca^{2+}$ overload in neostigmine-treated mice (28.87 ± 3.57%) and in SCS mice (25.51 ± 4.44%), and the nonspecific $IP_3R$ blocker, xestospongin (XS) reduced the endplate $Ca^{2+}$ overload in neostigmine-treated mice (26.15 ± 4.63%) and in SCS mice (22.85 ± 5.32%). Saline had no effect on endplate $Ca^{2+}$ overload (34.35 ± 2.11%); $n = 7$–10; ***$p < 0.001$. ***B***, Relative activity of calpain, caspase-3, and caspase-9 proteases (#, normalized to WT) for neostigmine-treated WT and untreated SCS muscle under indicated conditions. In non-pretreated WT mice neostigmine induced relative increases of protease activities of 3.3-fold (calpain), 2.5-fold (caspase-3), and 1.6-fold (caspase-9), while protease activities for nonn-pretreated SCS muscle are 4.2-fold (calpain), 2.7-fold (caspase-3), and 2.0-fold (caspase-9) above WT activity. siRNA treatment to silence $IP_3R_1$ significantly reduced calpain activity in neostigmine-treated mice (1.4-fold) and SCS mice (1.2-fold), caspase-3 activity in neostigmine-treated mice (1.3-fold) and SCS mice (1.8-fold), and caspase-9 activity in neostigmine-treated mice (1.1-fold) and SCS mice (1.2-fold). ctRNA had no effect in reducing protease activity. Treatment of SCS mice with XS significantly reduced activities of calpain mice (2.7-fold), caspase-3 mice (1.6-fold), and caspase-9 mice (1.5-fold). Treatment of SCS mice with 2-APB reduced activities of calpain mice (3.0-fold), caspase-3 mice (1.7-fold), and caspase-9 mice (1.6-fold); $n = 5$; *$p < 0.05$, **$p < 0.005$. ***C***, Top, Colocalization of activated caspase-3 (green, arrows) and caspase-9 (green, arrows) with NMJs (red) in WT, neostigmine-treated and non-pretreated SCS mice, and after $IP_3R_1$ knockdown. Activated caspase-3 and caspase-9 are seen in neostigmine-treated NMJ and in SCS NMJ with intact $IP_3R_1$, but are not seen in normal muscle and are significantly reduced in siRNA-treated NMJs; $n = 9$. Scale bar, 15 μm. Bottom, Quantitation of endplates labeled with activated caspase-3 and caspase-9 in neostigmine-treated and non-pretreated SCS mice under indicated conditions. In neostigmine-treated mice 28.2 ± 2.6% of endplates are labeled for cleaved caspase-3 and 25.4 ± 2.2% with active caspase-9, while in SCS mice 45.9 ± 5.0% are labeled with cleaved caspase-3 and 44.1 ± 5.7% with cleaved caspase-9. No active caspases were detected at untreated WT endplates. Treatment of TA muscle with siRNA for $IP_3R_1$ knockdown in neostigmine-treated mice significantly reduced labeling for cleaved caspase-3 (14.8 ± 0.9%) and caspase-9 (13.9 ± 2.0%), and in SCS mice it significantly reduced labeling for cleaved caspase-3 (14.8 ± 2.6%) and caspase-9 (15.7 ± 2.9%). ctRNA had no effect on labeling for cleaved caspase-3 and caspase-9. Treatment of SCS mice with XS significantly reduced endplate labeling with cleaved caspase-3 (25.1 ± 5.5%) and caspase-9 (27.5 ± 6.3%). Also, treatment of SCS mice with 2-APB significantly reduced endplate labeling with cleaved caspase-3 (28.2 ± 3.1%) and caspase-9 (24.8 ± 3.8%); $n = 5$; **$p < 0.005$. ***D***, $IP_3R_1$ activity is required for $Ca^{2+}$-mediated DNA damage in subsynaptic nuclei in SCS. Left, Colocalization of phospho-H2AX-labeled (pH2AX, green) nuclei (DAPI, blue) with NMJ (red) in untreated and staurosporine-treated WT muscle and untreated and siRNA-treated SCS muscle. After staurosporine treatment, nuclei throughout the muscle are labeled with pH2AX. In SCS only NMJ nuclei are labeled with pH2AX. In SCS muscle treated with siRNA for $IP_3R_1$ knockdown, pH2AX labeling of NMJ nuclei is reduced. Scale bar, 15 μm; Normal TA muscle sections were treated with staurosporine (800 μg/ml) at 37°C for 30 min (Rogakou et al., 2000). Right, Quantitation of pH2AX-labeled NMJs in WT and SCS under indicated conditions. In WT NMJ, pH2AX-labeled nuclei are rare (1.41 ± 1.23%). In SCS a significant number of NMJ nuclei are labeled with pH2AX (37.34 ± 2.17%). Pretreatment of SCS muscle with siRNA to knockdown $IP_3R_1$ (siRNA-SCS) significantly reduces $_{\gamma}$H2AX-labeling (11.42 ± 3.55%). ctRNA treatment (ctRNA-SCS) has no effect (35.58 ± 6.47%). Treatment of SCS mice with XS (XS-SCS) and 2-APB (2-APB-SCS) significantly reduce pH2AX-labeling to 20.52 ± 3.24 and 24.17 ± 1.67%, respectively; $n = 5$; **$p < 0.005$. All comparisons were analyzed by Mann–Whitney *U* test. All other comparisons not significant.

the nonspecific $IP_3R$ inhibitors 2-APB and XS also effectively decreased the proportion of pH2AX-labeled endplates in SCS mice to 24.2 ± 1.7 and 20.5 ± 3.2% (Fig. 5*D*; $n = 5$, $p < 0.005$), respectively. Collectively, these findings demonstrate that the $IP_3R_1$-mediated $Ca^{2+}$ release plays a significant role in mediating acute and chronic forms of synaptic $Ca^{2+}$ overload and the resulting activation of cysteine proteases at endplates and DNA damage in subsynaptic nuclei. Blockade or elimination of $IP_3R_1$ protects NMJs from these processes.

### $IP_3R_1$ silencing improves neuromuscular transmission and functional recovery in SCS transgenic mice

Weakness and fatigability in SCS and other NMJ disorders arise from impaired synaptic transmission manifested by decremental CMAP (compound muscle action potential) amplitudes with repetitive stimulation electromyography (rsEMG) and by combinations of presynaptic and postsynaptic defects as assessed using two-electrode voltage-clamp analysis of intact muscle *in vitro*. We performed rsEMG to investigate the role of $IP_3R_1$ in the impaired neuromuscular transmission and weakness induced in WT mice by anti-cholinesterase excess or that develops in untreated SCS mice (Laskowski and Dettbarn, 1979; Gomez et al., 1997). In mice with neuromuscular disease, decremental responses in the rsEMG are only detectable over the flexor digitorum brevis (FDB) muscle, presumably because of a high safety factor in most murine skeletal muscles (Schieppati et al., 1995; Corna et al., 1996). Thirty-six hours after intraperitoneal administration of neostigmine to WT mice, rsEMG revealed a mean decremental response of 10.6 ± 1.1% (Fig. 6; $n = 5$). However, when the FDB muscles on one side were pretreated by siRNA-mediated $IP_3R_1$ knockdown 9 d earlier, there was significant protection from neostigmine-induced decremental responses in rsEMG (5.6 ± 0.7%; $n = 5$, $p < 0.005$), while the treatment of contralateral FDB with control RNA had no effect on decremental responses (11.8 ± 1.2%; $n = 5$, $p > 0.95$). Similarly, untreated SCS mice showed mean decremental responses of 14.8 ± 1.4% (Fig. 6; $n = 5$) in the rsEMG. siRNA-mediated $IP_3R_1$ knockdown in FDB muscle diminished the decrement to 7.5 ± 1.1% ($n = 5$; $p < 0.005$), while control RNA had no effect (16.0 ± 1.0%; $n = 5$, $p > 0.83$). Lastly, treatment of SCS mice with the $IP_3R$ blocker 2-APB for 2 d significantly diminished decremental responses in SCS mice (8.0 ± 2.1%; $n = 5$, $p < 0.005$).

SCS mice have severely reduced MEPC amplitudes, MEPC frequency, and quantal content of evoked responses (Gomez et al., 1997). To investigate the physiological basis for the improvement in neuromuscular transmission induced by $IP_3R_1$ silencing in SCS mice, we used voltage-clamp analysis of endplate currents in excised TA muscle of SCS mice electroporated 9 d earlier with $IP_3R_1$-siRNA or control RNA (Fig. 7). As before, we found that both the amplitude and frequency of MEPCs were reduced, as was quantal content, in SCS mice (Gomez et al., 1997). Due to the expression of the mutant εL269F AChR subunit, MEPC decay phases were also prolonged, a finding that underlies the ionic overload leading to the disease process (Gomez et al., 1997). Surprisingly, upon treatment of TA muscle with $IP_3R_1$-siRNA we found that the MEPC amplitudes increased by 50% (1.63 ± 0.19 pA vs 1.1 ± 0.12 pA, $p < 0.03$; Fig. 7*B*), and the MEPC frequency was increased by >2-fold (1.75 ± 0.1 $s^{-1}$ vs 0.78 ± 0.04 $s^{-1}$, $p < 0.001$), and restored to the normal values (Fig. 7*A*, right). In contrast, MEPC amplitude and frequency in control RNA-treated SCS muscle remained reduced to levels similar to those seen in untreated SCS mice (Fig. 7*A*,*B*) and significantly lower than that seen in WT mice (Fig. 3*A*,*B*). In addition, in TA muscle

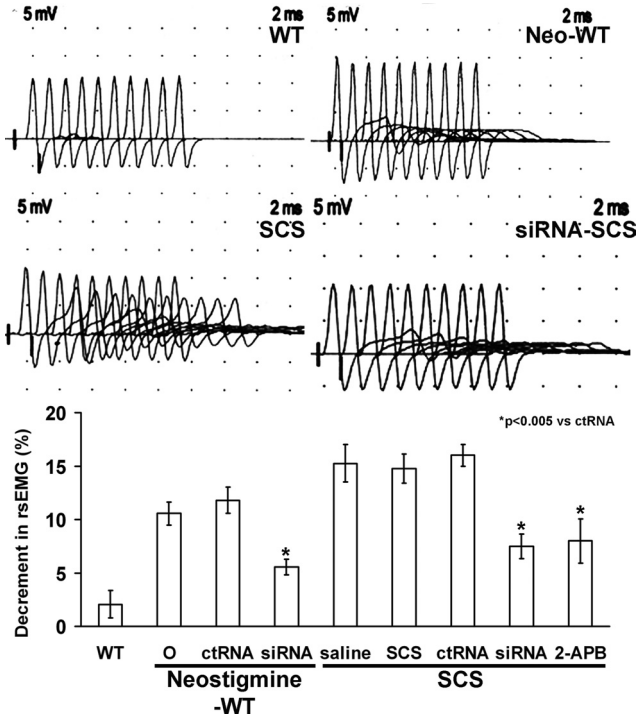


**Figure 6.** Decremental responses in rsEMG in SCS transgenic mouse and neostigmine myopathy depend on $IP_3R_1$ activity. Top, Compound muscle action potentials recorded during repetitive stimulation (rsEMG) in WT, neostigmine myopathy (Neo-WT), SCS, and SCS treated with siRNA to knockdown $IP_3R_1$. Decremental responses are seen in both SCS and Neo-WT. Bottom, Quantitation of decrement in rsEMG in WT, neostigmine myopathy, and SCS under indicated conditions. Decrement in WT rsEMG is only 2.06 ± 1.28% but is significantly increased in neostigmine myopathy (Neo-WT, 10.55 ± 1.12%) and SCS (14.75 ± 1.37%). $IP_3R_1$ silencing by siRNA reduces decrement to 5.55 ± 0.73% in neostigmine myopathy and 7.48 ± 1.14% in SCS. ctRNA had no effect in either condition. Blockade of $IP_3R_1$ by 2-APB reduced decrement to 8.00 ± 2.07%, while saline had no effect; $n = 5$; *$p < 0.005$, Mann–Whitney *U* test. All other comparisons not significant.

the amplitude of EPCs evoked by stimulating the corresponding tibialis nerve more than doubled in $IP_3R_1$-silenced SCS muscle (45.59 ± 6.45 vs 13.72 ± 2.8, $p < 0.003$) with RNA-treated or untreated SCS mice (Fig. 7*D*). The computed quantal content in $IP_3R_1$-silenced SCS TA muscle (Fig. 7*E*) was 28.03 ± 4.6, more than double that of control RNA-treated SCS muscle (12.55 ± 2.32, $p < 0.03$) and similar to normal TA muscle. Not surprisingly, MEPC decay time remained prolonged due to the continued expression of the mutant ε subunit (Gomez et al., 1997) (Fig. 3*C*). These results suggest that there is an overall restoration of both the presynaptic and postsynaptic defects in neuromuscular transmission in SCS mice by knockdown of the $IP_3R_1$ internal $Ca^{2+}$ store, which plays a key role in mediating the pathophysiological effects of the mutant AChRs in SCS. The fact that these parameters are improved without correcting the underlying kinetic defect in neuromuscular transmission indicates that the $IP_3R_1$ plays a key role in mediating the pathogenic effects of the mutant AChRs.

Mice with neuromuscular disease have impaired motor function, strength, and fatigue, as assessed by a variety measures of motor behavior (Gomez et al., 2002; Groshong et al., 2007). To investigate whether the single limb treatment paradigm led to improved motor performance, we used a computerized, video-assisted treadmill (DigiGait, MouseSpecifics), which allows side-by-side comparison of limb motor behavior using several hindlimb performance parameters including "brake time," "stride length," and "stride frequency" (defined in Materials and

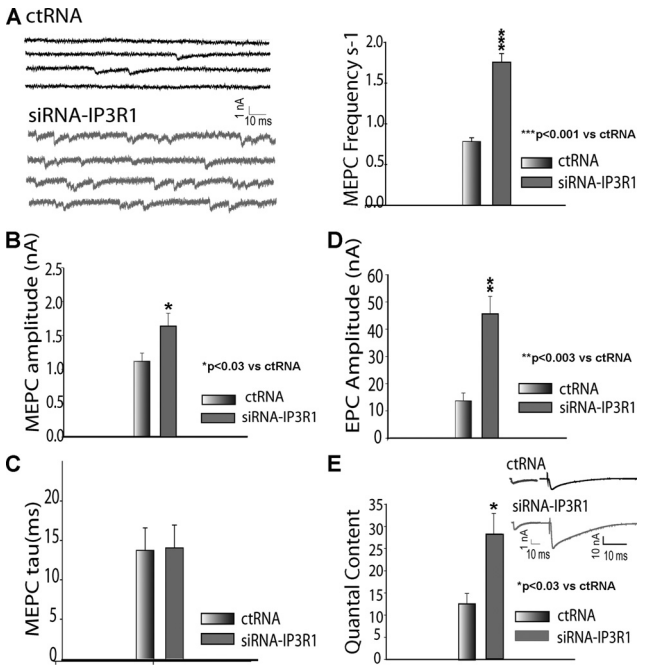


**Figure 7.** siRNA-mediated $IP_3R_1$ silencing alters SCS presynaptic and postsynaptic components of neuromuscular transmission. ***A***, Left, Representative traces of MEPCs in ctRNA-treated and siRNA-treated SCS mouse tibialis anterior muscle endplates, voltage clamped at −60 mV. Right, The frequency of spontaneous MEPC was significantly increased in $IP_3R_1$-siRNA-treated muscle ($n = 20$) compared with ctRNA-treated TA ($n = 19$) ($1.75 \pm 0.1\ s^{-1}$ vs $0.78 \pm 0.04\ s^{-1}$, ***$p < 0.001$). ***B***, MEPC amplitudes from $IP_3R_1$-siRNA-treated SCS TA muscle ($1.63 \pm 0.19$, $n = 20$) were nearly 47% greater than those recorded from ctRNA-treated SCS TA muscle ($1.11 \pm 0.12$, $n = 10$; *$p < 0.03$). ***C***, The MEPC ($\tau$) in $IP_3R_1$-siRNA-treated TA ($14.04 \pm 2.89$ ms, $n = 13$) remained prolonged and unchanged compared with that of ctRNA-treated SCS, consistent with the presence of the SCS mutation εL269F ($13.72 \pm 2.85$ ms, $n = 7$). ***D***, EPC amplitude of $IP_3R_1$-siRNA-treated TA muscle ($n = 13$) was significantly greater than that of the ctRNA-treated muscle ($45.59 \pm 6.45$ nA; $n = 13$ vs $13.72 \pm 2.8$ nA; $n = 7$; **$p < 0.003$). ***E***, The computed quantal content of evoked transmitter release was nearly doubled in $IP_3R_1$-siRNA-treated SCS TA muscle compared with ctRNA-treated muscle ($28.3 \pm 4.6$; $n = 13$ vs $12.55 \pm 2.32$; $n = 7$, *$p < 0.03$). Inset shows average traces of MEPC and EPC for $IP_3R_1$-siRNA-treated and ctRNA-treated SCS endplates; $n$ = # of endplates. Mouse # = 4. All comparisons were analyzed by Student's *t* test. All other comparisons not significant.

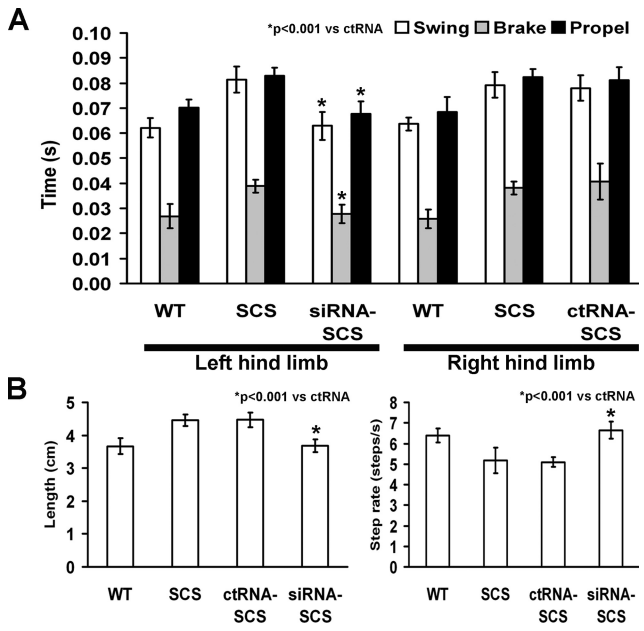


**Figure 8.** $IP_3R_1$ silencing improves motor function in SCS mice. ***A***, Hindlimb motor time interval parameters measured in motorized treadmill (DigiGait) in WT and SCS mice and the effect of unilateral $IP_3R_1$ silencing. Functional parameters termed "swing", "brake", and "propel" are time intervals for three components of normal leg movements recorded during walking; as defined in Materials and Methods, these are identical between left and right hindlimb in WT mice. All three parameters are symmetrically and significantly increased in SCS mice. siRNA treatment of left hindlimb TA causes significant improvement in each of these parameters in comparison to the contralateral right hindlimb, which was treated with ctRNA; $n = 11$; *$p <$ 0.001, Student's *t* test. All other comparisons not significant. ***B***, Mean hindlimb stride length and step frequency in WT and SCS and the effect of unilateral $IP_3R_1$ silencing. The average stride length for both limbs in SCS is significantly longer than WT, while the step frequency is lower. siRNA treatment of the left TA of the SCS mice reduced the stride length to that of WT and increased the step frequency to slightly greater than that of WT; $n = 11$; *$p < 0.001$, Student's *t* test. All other comparisons not significant.

Methods). Each of these was significantly prolonged in SCS mice (Fig. 8*A*). However, treatment of one TA with siRNA-$IP_3R_1$ and the opposite TA with control RNA led to a significant improvement in all three parameters in siRNA-treated SCS limb compared with the control RNA-treated SCS limb (Fig. 8*A*). In untreated SCS mice, stride length was 4.5 cm compared with 3.7 cm in WT mice (Fig. 8*B*; $n = 11$, $p < 0.001$). In the siRNA-IP3R1-treated side the mean stride length was 3.6 cm while the control RNA-treated side was 4.6 cm ($n = 1$,; $p < 0.001$). Mean stride frequency in SCS mice was $5.2\ s^{-1}$ compared with $6.4\ s^{-1}$ in WT mice (Fig. 8B; $n = 11$; $p < 0.001$). In siRNA-treated hindlimb, the mean stride frequency was $6.7\ s^{-1}$ compared with $5.1\ s^{-1}$ in control RNA limb ($n = 11$, $p < 0.001$). These findings further demonstrate the importance of the $IP_3R_1$ in mediating the full spectrum of histochemical, pathological, electrophysiological, and clinical consequences arising from pharmacological or genetic perturbation of AChR gating in neuromuscular disorders.

## Discussion

In skeletal muscle fibers many developmental and physiological processes depend on $Ca^{2+}$ fluxes associated with cholinergic input. The NMJ is the site of transient increases in sarcoplasmic $Ca^{2+}$ distinct from other $Ca^{2+}$ fluxes in muscle that, until now, were attributed to the permeability of the AChR to $Ca^{2+}$ (Miledi et al., 1980; Goldman et al., 1988; Decker and Dani, 1990; Villarroel and Sakmann, 1996; Fucile et al., 2006). We previously used living, fura-2-loaded muscle fibers focally activated at the NMJ with iontophoresed ACh to show that localized increases in NMJ $Ca^{2+}$ to both normal and pathological levels could be inhibited by blocking $IP_3Rs$ or $IP_3$ production (Zayas et al., 2007). Initial increases in $Ca^{2+}$ still presumably occur by entry through WT or mutant AChRs (Zayas et al., 2007). $IP_3$ is produced by the action of phospholipase C activated by G protein-coupled receptors such as muscarinic receptors (Furlan and Godinho, 2005; Garcia et al., 2005; Wright et al., 2009). In the current study we identified the responsible $IP_3R$ subtype as $IP_3R_1$ and demonstrated for the first time that $IP_3R_1s$ are required for critical developmental and physiological processes at the NMJ, ranging from the earliest events of AChR cluster dispersal in developing myotubes to homeostatic plasticity and the control of synaptic gene expression in innervated fibers. Furthermore, we found that in adult fibers $IP_3R_1s$ also underlie pathological conditions of focal synaptic $Ca^{2+}$ overload, which are prevented by $IP_3R$ blockade or $IP_3R_1$ knockdown.

The findings in this study are significant for several reasons. First, they reveal a novel role for $IP_3R_1$ in enabling the signaling required for early maturation of the NMJ, presumably by amplifying agonist-evoked $Ca^{2+}$ signals at the AChR clusters to accelerate cluster dispersal. No comparable role for $IP_3R_1$ in other neuronal cell types has been demonstrated. Second, the findings

in mature NMJs suggest that this novel role is expanded in formed synapses to provide an additional mechanism by which localized neural signals may be transduced efficiently into $Ca^{2+}$ store release. This expanded role influences presynaptic and postsynaptic homeostatic synaptic plasticity and changes in synaptic gene expression, yet remains compartmentalized at the muscle fiber synapse. Third, they show that this internal $Ca^{2+}$ release store is a significant source of pathological elevations of $Ca^{2+}$ and therefore a potential target for therapy in disorders mediated by $Ca^{2+}$ overload, such as excitotoxicity, without apparent adverse effects in the fully formed synapse.

The importance of $IP_3R_1$ in early NMJ development is consistent with the previous observation that ACh mobilizes internal $Ca^{2+}$ in C2C12 cells and the critical finding that agonist-mediated cluster dispersal depends on activation of calpain (Giovannelli et al., 1995; Chen et al., 2007). $IP_3R_1$ expression appears in embryonic development and, based on the presence of an E-box motif in the ITPR1 gene promoter, likely exhibits coordinate regulation with other muscle genes by myogenic regulatory factors (Konishi et al., 1997; Yafe et al., 2008). The basis for its predominant localization at the NMJ has yet to be explained.

Increases in quantal transmitter release and AChR expression in innervated muscle fibers induced by partial blockade of neuromuscular transmission reflect the property of homeostatic plasticity (Gallego et al., 1979; Domet et al., 1995; Wang et al., 2005, 2010). Our findings that these changes can be mimicked by $IP_3R_1$ silencing suggest that they may occur through the intracellular $Ca^{2+}$ release via $IP_3R_1$.

The selective role of $IP_3R_1$ activity on gene expression at the NMJ can be partially explained by the localized effect of $IP_3R_1$ silencing or inhibition on HDAC4 translocation into myonuclei at the NMJ (Cohen et al., 2007). Reducing intracellular $Ca^{2+}$ by siRNA-mediated $IP_3R_1$ knockdown may diminish $Ca^{2+}$-dependent CaMKII activity, which leads to reduction in CaMKII-mediated phosphorylation of HDAC4. HDAC4 must be phosphorylated to be exported from nuclei, and thus accumulates in nuclei (Backs et al., 2006; Cohen et al., 2007). This is consistent with our immunostaining results of intense localization of HDAC4 in subsynaptic myonuclei in $IP_3R_1$ knockdown in TA muscle, which was similar to but more localized than the widespread accumulation of HDAC4 in myonuclei after denervation. Many of the effects of muscle denervation on gene expression may act through HDAC4, which suppresses the transcriptional corepressor Dach2 and allows expression of myogenin and downstream E-box-containing NMJ genes (Tang et al., 2004). Thus, the changes in gene expression after siRNA silencing of $IP_3R_1$ may result from a similar although more NMJ-localized action of HDAC4 on gene expression. The increased expression of ErbB2, the neuregulin receptor in intact synapses, may provide an additional positive feedback for increased AChR expression (Méjat et al., 2003).

Denervation and $IP_3R_1$ silencing do not have identical effects on NMJ gene expression. Clearly, numerous other neural factors such as agrin and neuregulin, as well as sarcolemmal electrical activity, may also play roles in modulating gene expression and are likely to persist in intact NMJs after $IP_3R_1$ silencing (Goldman et al., 1988; Lebrasseur et al., 2003; Weston et al., 2007). In some cases, combined denervation and $IP_3R_1$ silencing were similar or additive to single treatments, suggesting similar pathways, while other cases, such as the greater effect of denervation on rapsyn and the opposing effect on AChE expression, suggest that polypeptide neural factors may play a greater role in controlling expression of these genes. On the other hand, $IP_3R_1$ silencing had a greater effect on expression of the $\varepsilon$ subunit and particularly ErbB2, suggesting that either the expression of these genes is coordinately regulated or that they act in the same pathway.

These studies provide a detailed description of the role of muscle $IP_3R_1$ and compartmentalized $Ca^{2+}$ signals at the NMJ in coordinating synaptic processes. Given the differences in expression patterns and levels of $IP_3R$ in different cells and the diverse and severe phenotypes of spontaneous and induced mutations, it is likely that $IP_3Rs$ have very cell-specific functions (Matsumoto et al., 1996; Acharya et al., 1997; Inoue et al., 1998; Itoh et al., 2001). Thus, these findings will require further study in other systems to be able to extrapolate to other cell types.

While our findings in developing muscle suggest that elimination of $IP_3R_1$ in embryonic muscle might adversely affect the development of synapses, we find that $IP_3R_1$ antagonism in adult innervated muscle, while playing a key role in function, may only qualitatively affect synaptic function through refining of synaptic gene expression and homeostatic regulation of synaptic transmission. Thus, therapy directed at reducing $IP_3R_1$ activity may be well tolerated as a therapeutic strategy for excitotoxic conditions or conditions of $Ca^{2+}$ overload, such as muscular dystrophy (Mondin et al., 2009).

Deranged intracellular $Ca^{2+}$ release through $IP_3Rs$ has been implicated in the pathogenesis of other muscle and neuronal degenerative disorders (Monnier et al., 2000; Bezprozvanny, 2011). We studied two neuromuscular conditions whose pathogeneses are directly related to synaptic (NMJ) $Ca^{2+}$ overload, anticholinesterase excess, and the slow-channel myasthenic syndrome (Engel et al., 1977, 1998; Gomez et al., 1997). As suggested by our previous *in vitro* single muscle cell study, $IP_3R_1$ silencing *in vivo* completely eliminated synaptic $Ca^{2+}$ overload in both conditions. Subacute blockade of $IP_3R$ in SCS transgenic mice using XS and 2-APB was also effective at eliminating NMJ $Ca^{2+}$ overload. Moreover, these treatments were effective at interrupting the pathological cascade in the NMJ that includes activation of cysteine proteases, damage to subsynaptic double strand DNA, and physiological and clinical impairment of neuromuscular transmission. Thus, $IP_3R_1$ antagonism in this study had a dramatic effect at reducing pathologic changes and protecting the NMJ in two conditions of cholinergic excess. These studies suggest that studies directed at modulating this intracellular $Ca^{2+}$ release pathway in neurodegenerative or excitotoxic conditions may be neuroprotective and well tolerated.

## References

Acharya JK, Jalink K, Hardy RW, Hartenstein V, Zuker CS (1997) InsP3 receptor is essential for growth and differentiation but not for vision in *Drosophila*. Neuron 18:881–887.

Akaaboune M, Culican SM, Turney SG, Lichtman JW (1999) Rapid and reversible effects of activity on acetylcholine receptor density at the neuromuscular junction in vivo. Science 286:503–507.

Ariens AT, Cohen EM, Meeter E, Wolthuis OL (1968) Reversible necrosis in striated muscle fibres of the rat after severe intoxication with various cholinesterase inhibitors. IMS Ind Med Surg 37:845–847.

Backs J, Song K, Bezprozvannaya S, Chang S, Olson EN (2006) CaM kinase II selectively signals to histone deacetylase 4 during cardiomyocyte hypertrophy. J Clin Invest 116:1853–1864.

Belmokhtar CA, Hillion J, Ségal-Bendirdjian E (2001) Staurosporine induces apoptosis through both caspase-dependent and caspase-independent mechanisms. Oncogene 20:3354–3362.

Berridge MJ, Irvine RF (1984) Inositol trisphosphate, a novel second messenger in cellular signal transduction. Nature 312:315–321.

Bezprozvanny I (2011) Role of inositol 1,4,5-trisphosphate receptors in pathogenesis of Huntington's disease and spinocerebellar ataxias. Neurochem Res 36:1186–1197.

Bhattacharyya BJ, Day JW, Gundeck JE, Leonard S, Wollmann RL, Gomez

CM (1997) Desensitization of mutant acetylcholine receptors in transgenic mice reduces the amplitude of neuromuscular synaptic currents. Synapse 27:367–377.

Boehning D, Patterson RL, Sedaghat L, Glebova NO, Kurosaki T, Snyder SH (2003) Cytochrome *c* binds to inositol (1,4,5) trisphosphate receptors, amplifying calcium-dependent apoptosis. Nat Cell Biol 5:1051–1061.

Bootman MD, Collins TJ, Mackenzie L, Roderick HL, Berridge MJ, Peppiatt CM (2002) 2-Aminoethoxydiphenyl borate (2-APB) is a reliable blocker of store-operated $Ca^{2+}$ entry but an inconsistent inhibitor of $InsP_3$-induced $Ca^{2+}$ release. FASEB J 16:1145–1150.

Carlson CG, Kriebel ME (1985) Neostigmine increases the size of subunits composing the quantum of transmitter release at mouse neuromuscular junction. J Physiol 367:489–502.

Castelló A, Cadefau J, Cussó R, Testar X, Hesketh JE, Palacín M, Zorzano A (1993) GLUT-4 and GLUT-1 glucose transporter expression is differentially regulated by contractile activity in skeletal muscle. J Biol Chem 268:14998–15003.

Chen F, Qian L, Yang ZH, Huang Y, Ngo ST, Ruan NJ, Wang J, Schneider C, Noakes PG, Ding YQ, Mei L, Luo ZG (2007) Rapsyn interaction with calpain stabilizes AChR clusters at the neuromuscular junction. Neuron 55:247–260.

Choi DW (1992) Excitotoxic cell death. J Neurobiol 23:1261–1276.

Choi DW (1995) Calcium: still center-stage in hypoxic-ischemic neuronal death. Trends Neurosci 18:58–60.

Cohen TJ, Waddell DS, Barrientos T, Lu Z, Feng G, Cox GA, Bodine SC, Yao TP (2007) The histone deacetylase HDAC4 connects neural activity to muscle transcriptional reprogramming. J Biol Chem 282:33752–33759.

Corna S, Galante M, Grasso M, Nardone A, Schieppati M (1996) Unilateral displacement of lower limb evokes bilateral EMG responses in leg and foot muscles in standing humans. Exp Brain Res 109:83–91.

Decker ER, Dani JA (1990) Calcium permeability of the nicotinic acetylcholine receptor: the single-channel calcium influx is significant. J Neurosci 10:3413–3420.

Demuro A, Parker I, Stutzmann GE (2010) Calcium signaling and amyloid toxicity in Alzheimer disease. J Biol Chem 285:12463–12468.

Domet MA, Webb CE, Wilson DF (1995) Impact of alpha-bungarotoxin on transmitter release at the neuromuscular junction of the rat. Neurosci Lett 199:49–52.

Engel AG, Lambert EH, Gomez MR (1977) A new myasthenic syndrome with end-plate acetylcholinesterase deficiency, small nerve terminals, and reduced acetylcholine release. Ann Neurol 1:315–330.

Engel AG, Ohno K, Milone M, Wang HL, Nakano S, Bouzat C, Pruitt JN 2nd, Hutchinson DO, Brengman JM, Bren N, Sieb JP, Sine SM (1996) New mutations in acetylcholine receptor subunit genes reveal heterogeneity in the slow-channel congenital myasthenic syndrome. Hum Mol Genet 5:1217–1227.

Engel AG, Ohno K, Milone M, Sine SM (1998) Congenital myasthenic syndromes. New insights from molecular genetic and patch-clamp studies. Ann N Y Acad Sci 841:140–156.

Engel AG, Shen XM, Selcen D, Sine SM (2010) What have we learned from the congenital myasthenic syndromes. J Mol Neurosci 40:143–153.

Friedrich O, von Wegner F, Chamberlain JS, Fink RH, Rohrbach P (2008) L-type $Ca^{2+}$ channel function is linked to dystrophin expression in mammalian muscle. PLoS One 3:e1762.

Fucile S, Sucapane A, Grassi F, Eusebi F, Engel AG (2006) The human adult subtype ACh receptor channel has high $Ca^{2+}$ permeability and predisposes to endplate $Ca^{2+}$ overloading. J Physiol 573:35–43.

Furlan I, Godinho RO (2005) Developing skeletal muscle cells express functional muscarinic acetylcholine receptors coupled to different intracellular signaling systems. Br J Pharmacol 146:389–396.

Furuichi T, Shiota C, Mikoshiba K (1990) Distribution of inositol 1,4,5-trisphosphate receptor mRNA in mouse tissues. FEBS Lett 267:85–88.

Galeotti N, Bartolini A, Ghelardini C (2006) Blockade of intracellular calcium release induces an antidepressant-like effect in the mouse forced swimming test. Neuropharmacology 50:309–316.

Gallego R, Kuno M, Núñez R, Snider WD (1979) Disuse enhances synaptic efficacy in spinal mononeurones. J Physiol 291:191–205.

Garcia N, Santafé MM, Salon I, Lanuza MA, Tomàs J (2005) Expression of muscarinic acetylcholine receptors (M1-, M2-, M3- and M4-type) in the neuromuscular junction of the newborn and adult rat. Histol Histopathol 20:733–743.

Giovannelli A, Grassi F, Limatola C, Mattei E, Ragozzino D, Eusebi F (1995) Acetylcholine-activated inward current induces cytosolic $Ca^{2+}$ mobilization in mouse C2C12 myotubes. Cell Calcium 18:41–50.

Goldman D, Brenner HR, Heinemann S (1988) Acetylcholine receptor alpha-, beta-, gamma-, and delta-subunit mRNA levels are regulated by muscle activity. Neuron 1:329–333.

Golzio M, Mazzolini L, Moller P, Rols MP, Teissié J (2005) Inhibition of gene expression in mice muscle by in vivo electrically mediated siRNA delivery. Gene Ther 12:246–251.

Gomez CM, Maselli R, Gundeck JE, Chao M, Day JW, Tamamizu S, Lasalde JA, McNamee M, Wollmann RL (1997) Slow-channel transgenic mice: a model of postsynaptic organellar degeneration at the neuromuscular junction. J Neurosci 17:4170–4179.

Gomez CM, Maselli R, Williams JM, Bhattacharyya BB, Wollmann RL, Day JW (1998) Genetic manipulation of AChR responses suggests multiple causes of weakness in slow-channel syndrome. Ann N Y Acad Sci 841:167–180.

Gomez CM, Maselli RA, Groshong J, Zayas R, Wollmann RL, Cens T, Charnet P (2002) Active calcium accumulation underlies severe weakness in a panel of mice with slow-channel syndrome. J Neurosci 22:6447–6457.

Gómez-Sintes R, Lucas JJ (2010) NFAT/Fas signaling mediates the neuronal apoptosis and motor side effects of GSK-3 inhibition in a mouse model of lithium therapy. J Clin Invest 120:2432–2445.

Groshong JS, Spencer MJ, Bhattacharyya BJ, Kudryashova E, Vohra BP, Zayas R, Wollmann RL, Miller RJ, Gomez CM (2007) Calpain activation impairs neuromuscular transmission in a mouse model of the slow-channel myasthenic syndrome. J Clin Invest 117:2903–2912.

Hampton TG, Stasko MR, Kale A, Amende I, Costa AC (2004) Gait dynamics in trisomic mice: quantitative neurological traits of Down syndrome. Physiol Behav 82:381–389.

Holland RL, Brown MC (1980) Postsynaptic transmission block can cause terminal sprouting of a motor nerve. Science 207:649–651.

Ikeda SR, Aronstam RS, Daly JW, Aracava Y, Albuquerque EX (1984) Interactions of bupivacaine with ionic channels of the nicotinic receptor. Electrophysiological and biochemical studies. Mol Pharmacol 26:293–303.

Inoue T, Kato K, Kohda K, Mikoshiba K (1998) Type 1 inositol 1,4,5-trisphosphate receptor is required for induction of long-term depression in cerebellar Purkinje neurons. J Neurosci 18:5366–5373.

Itoh S, Ito K, Fujii S, Kaneko K, Kato K, Mikoshiba K, Kato H (2001) Neuronal plasticity in hippocampal mossy fiber-CA3 synapses of mice lacking the inositol-1,4,5-trisphosphate type 1 receptor. Brain Res 901:237–246.

Jones JP, Tapscott EB, Olson AL, Pessin JE, Dohm GL (1998) Regulation of glucose transporters GLUT-4 and GLUT-1 gene transcription in denervated skeletal muscle. J Appl Physiol 84:1661–1666.

Kashiwa HK, House CM Jr (1964) The glyoxal bis(2-hydroxyanil) method modified for localizing insoluble calcium salts. Stain Technol 39:359–367.

Kawabuchi M (1982) Neostigmine myopathy is a calcium ion-mediated myopathy initially affecting the motor end-plate. J Neuropathol Exp Neurol 41:298–314.

Kobayashi S, Yano M, Suetomi T, Ono M, Tateishi H, Mochizuki M, Xu X, Uchinoumi H, Okuda S, Yamamoto T, Koseki N, Kyushiki H, Ikemoto N, Matsuzaki M (2009) Dantrolene, a therapeutic agent for malignant hyperthermia, markedly improves the function of failing cardiomyocytes by stabilizing interdomain interactions within the ryanodine receptor. J Am Coll Cardiol 53:1993–2005.

Koelle GB, Friedenwald JA (1949) A histochemical method for localizing cholinesterase activity. Proc Soc Exp Biol Med 70:617–622.

Konishi Y, Kobayashi Y, Kishimoto T, Makino Y, Miyawaki A, Furuichi T, Okano H, Mikoshiba K, Tamura T (1997) Demonstration of an E-box and its CNS-related binding factors for transcriptional regulation of the mouse type 1 inositol 1,4,5-trisphosphate receptor gene. J Neurochem 69:476–484.

Laskowski MB, Dettbarn WD (1979) An electrophysiological analysis of the effects of paraoxon at the neuromuscular junction. J Pharmacol Exp Ther 210:269–274.

Lebrasseur NK, Coté GM, Miller TA, Fielding RA, Sawyer DB (2003) Regulation of neuregulin/ErbB signaling by contractile activity in skeletal muscle. Am J Physiol Cell Physiol 284:C1149–C1155.

Lee SG, Su ZZ, Emdad L, Sarkar D, Franke TF, Fisher PB (2008) Astrocyte elevated gene-1 activates cell survival pathways through PI3K-Akt signaling. Oncogene 27:1114–1121.

Leonard JP, Salpeter MM (1979) Agonist-induced myopathy at the neuromuscular junction is mediated by calcium. J Cell Biol 82:811–819.

Lømo T, Massoulié J, Vigny M (1985) Stimulation of denervated rat soleus muscle with fast and slow activity patterns induces different expression of acetylcholinesterase molecular forms. J Neurosci 5:1180–1187.

Marks AR (1997) Intracellular calcium-release channels: regulators of cell life and death. Am J Physiol 272:H597–H605.

Martinou JC, Merlie JP (1991) Nerve-dependent modulation of acetylcholine receptor epsilon-subunit gene expression. J Neurosci 11:1291–1299.

Matsumoto M, Nakagawa T, Inoue T, Nagata E, Tanaka K, Takano H, Minowa O, Kuno J, Sakakibara S, Yamada M, Yoneshima H, Miyawaki A, Fukuuchi Y, Furuichi T, Okano H, Mikoshiba K, Noda T (1996) Ataxia and epileptic seizures in mice lacking type 1 inositol 1,4,5-trisphosphate receptor. Nature 379:168–171.

Megeath LJ, Fallon JR (1998) Intracellular calcium regulates agrin-induced acetylcholine receptor clustering. J Neurosci 18:672–678.

Méjat A, Ravel-Chapuis A, Vandromme M, Schaeffer L (2003) Synapse-specific gene expression at the neuromuscular junction. Ann N Y Acad Sci 998:53–65.

Miledi R, Parker I, Schalow G (1980) Transmitter induced calcium entry across the postsynaptic membrane at frog end-plates measured using arsenazo III. J Physiol 300:197–212.

Mondin L, Balghi H, Constantin B, Cognard C, Sebille S (2009) Negative modulation of inositol 1,4,5-trisphosphate type 1 receptor expression prevents dystrophin-deficient muscle cells death. Am J Physiol Cell Physiol 297:C1133–C1145.

Monnier N, Romero NB, Lerale J, Nivoche Y, Qi D, MacLennan DH, Fardeau M, Lunardi J (2000) An autosomal dominant congenital myopathy with cores and rods is associated with a neomutation in the RYR1 gene encoding the skeletal muscle ryanodine receptor. Hum Mol Genet 9:2599–2608.

Moore C, Leu M, Müller U, Brenner HR (2001) Induction of multiple signaling loops by MuSK during neuromuscular synapse formation. Proc Natl Acad Sci U S A 98:14655–14660.

Mulder KJ, Mulder JB (1979) Ketamine and xylazine anesthesia in the mouse. Vet Med Small Anim Clin 74:569–570.

Murthy VN, Schikorski T, Stevens CF, Zhu Y (2001) Inactivity produces increases in neurotransmitter release and synapse size. Neuron 32:673–682.

Plomp JJ, van Kempen GT, Molenaar PC (1992) Adaptation of quantal content to decreased postsynaptic sensitivity at single endplates in alpha-bungarotoxin-treated rats. J Physiol 458:487–499.

Powell JA, Molgó J, Adams DS, Colasante C, Williams A, Bohlen M, Jaimovich E (2003) IP3 receptors and associated $Ca^{2+}$ signals localize to satellite cells and to components of the neuromuscular junction in skeletal muscle. J Neurosci 23:8185–8192.

Rogakou EP, Nieves-Neira W, Boon C, Pommier Y, Bonner WM (2000) Initiation of DNA fragmentation during apoptosis induces phosphorylation of H2AX histone at serine 139. J Biol Chem 275:9390–9395.

Ross CA, Danoff SK, Schell MJ, Snyder SH, Ullrich A (1992) Three additional inositol 1,4,5-trisphosphate receptors: molecular cloning and differential localization in brain and peripheral tissues. Proc Natl Acad Sci U S A 89:4265–4269.

Schertzer JD, Plant DR, Lynch GS (2006) Optimizing plasmid-based gene transfer for investigating skeletal muscle structure and function. Mol Ther 13:795–803.

Schieppati M, Nardone A, Siliotto R, Grasso M (1995) Early and late stretch responses of human foot muscles induced by perturbation of stance. Exp Brain Res 105:411–422.

Streb H, Irvine RF, Berridge MJ, Schulz I (1983) Release of $Ca^{2+}$ from a nonmitochondrial intracellular store in pancreatic acinar cells by inositol-1,4,5-trisphosphate. Nature 306:67–69.

Sugiyama JE, Glass DJ, Yancopoulos GD, Hall ZW (1997) Laminin-induced acetylcholine receptor clustering: an alternative pathway. J Cell Biol 139:181–191.

Sunesen M, Changeux JP (2003) Transcription in neuromuscular junction formation: who turns on whom? J Neurocytol 32:677–684.

Tang H, Macpherson P, Argetsinger LS, Cieslak D, Suhr ST, Carter-Su C, Goldman D (2004) CaM kinase II-dependent phosphorylation of myogenin contributes to activity-dependent suppression of nAChR gene expression in developing rat myotubes. Cell Signal 16:551–563.

Thiermann H, Zilker T, Eyer F, Felgenhauer N, Eyer P, Worek F (2009) Monitoring of neuromuscular transmission in organophosphate pesticide-poisoned patients. Toxicol Lett 191:297–304.

Tsay HJ, Schmidt J (1989) Skeletal muscle denervation activates acetylcholine receptor genes. J Cell Biol 108:1523–1526.

Villarroel A, Sakmann B (1996) Calcium permeability increase of end-plate channels in rat muscle during postnatal development. J Physiol 496:331–338.

Vohra BP, Groshong JS, Maselli RA, Verity MA, Wollmann RL, Gomez CM (2004) Focal caspase activation underlies the endplate myopathy in slow-channel syndrome. Ann Neurol 55:347–352.

Vohra BP, Groshong JS, Zayas R, Wollmann RL, Gomez CM (2006) Activation of apoptotic pathways at muscle fiber synapses is circumscribed and reversible in a slow-channel syndrome model. Neurobiol Dis 23:462–470.

Wang X, Li Y, Engisch KL, Nakanishi ST, Dodson SE, Miller GW, Cope TC, Pinter MJ, Rich MM (2005) Activity-dependent presynaptic regulation of quantal size at the mammalian neuromuscular junction in vivo. J Neurosci 25:343–351.

Wang X, Pinter MJ, Rich MM (2010) $Ca^{2+}$ dependence of the binomial parameters p and n at the mouse neuromuscular junction. J Neurophysiol 103:659–666.

Wells DJ (2004) Gene therapy progress and prospects: electroporation and other physical methods. Gene Ther 11:1363–1369.

Weston CA, Teressa G, Weeks BS, Prives J (2007) Agrin and laminin induce acetylcholine receptor clustering by convergent, Rho GTPase-dependent signaling pathways. J Cell Sci 120:868–875.

Wilson SM, Bhattacharyya B, Rachel RA, Coppola V, Tessarollo L, Householder DB, Fletcher CF, Miller RJ, Copeland NG, Jenkins NA (2002) Synaptic defects in ataxia mice result from a mutation in Usp14, encoding a ubiquitin-specific protease. Nat Genet 32:420–425.

Wright MC, Potluri S, Wang X, Dentcheva E, Gautam D, Tessler A, Wess J, Rich MM, Son YJ (2009) Distinct muscarinic acetylcholine receptor subtypes contribute to stability and growth, but not compensatory plasticity, of neuromuscular synapses. J Neurosci 29:14942–14955.

Yafe A, Shklover J, Weisman-Shomer P, Bengal E, Fry M (2008) Differential binding of quadruplex structures of muscle-specific genes regulatory sequences by MyoD, MRF4 and myogenin. Nucleic Acids Res 36:3916–3925.

Yang JS, Sladky JT, Kallen RG, Barchi RL (1991) TTX-sensitive and TTX-insensitive sodium channel mRNA transcripts are independently regulated in adult skeletal muscle after denervation. Neuron 7:421–427.

Zayas R, Groshong JS, Gomez CM (2007) Inositol-1,4,5-triphosphate receptors mediate activity-induced synaptic $Ca^{2+}$ signals in muscle fibers and $Ca^{2+}$ overload in slow-channel syndrome. Cell Calcium 41:343–352.

Zhu DL, Peng HB (1988) Increase in intracellular calcium induced by the polycation-coated latex bead, a stimulus that causes postsynaptic-type differentiation in cultured *Xenopus* muscle cells. Dev Biol 126:63–70.